3.0 EMISSIONS REDUCTION

The objective of this task was to extend the studies of emissions from coal-fired industrial boilers that were conducted in the first two phases of the project. The activities that were performed involved fundamental studies, pilot-scale investigations, and full-scale demonstrations and included:

- Evaluations of NO_x reduction strategies such as low-temperature selective catalytic reduction and reburning by injecting a biomass-based product and a micronized coal-water mixture;
- A pilot-scale investigation of simultaneous SO_2 removal/NO_x reduction technology injecting a biomass-based product of pyrolysis in the combustion chamber;
- A fundamental study of formation/destruction mechanisms of polycyclic aromatic hydrocarbons followed by demonstration-scale testing;
- Comprehensive studies of trace elements and mercury emissions investigating the effect of coal cleaning, particulate removal devices, and operating conditions on trace element emissions;
- The development of a Unified Methodology for simultaneously measuring trace element emissions and mercury speciation;
- Continuing the investigation of fine particulate matter removal using ceramic filters; and
- The development of a novel molecular basket to capture CO_2 emissions from the flue gas of coal-fired boilers.

Each of these activities is discussed in detail in the following sections. Some of the activities expanded upon work that began in Phase II, which has been reported previously (Miller et al., 2000).

3.1 NO_x Reduction/ SO_2 Removal

In this activity, NO_x reduction and SO_2 removal strategies were investigated. NO_x reduction was investigated using low-temperature, selective catalytic reduction (SCR), BioLime^{TM} injection was studied for simultaneous NO_x/SO_2 control, and reburning tests for NO_x control were conducted. Sorbent injection tests were originally planned for SO_2/SO_3 control (as part of the low-temperature SCR work); however, the sorbent injection results from Phase II were so successful, with up to 98% SO_2 capture observed, that DOE and Penn State agreed not to pursue this work any further (Miller et al., 2000).

3.1.1 Low-Temperature Selective Catalytic Reduction

A low-temperature SCR activity was initiated in Phase II and extended into the Phase III of the project. The overall objectives for the low-temperature SCR activity were to:

1) To identify and/or develop a NO_x reduction catalyst that is compatible with the typical operating conditions and the economic constraints of industrial boilers, specifically:
    - Flue gas temperatures of 550°F (288°C);
    - O_2 concentrations of 3-5 vol.%;
    - H_2O concentration of 10-20 vol.%;
    - SO_2 concentrations of 500-1,000 ppm;
    - NO concentrations of 100-500 ppm;
    - No regeneration of sorbent/catalyst required; and
    - Low maintenance and operating costs.
2) To establish the limitations of the candidate NO_x reduction catalyst so that its implementation in pilot and demonstration-scale tests will be straightforward, for example, determining the relationship between space velocity and NO_x conversion efficiency for scale-up purposes.
3) To identify maximum allowable transients that the catalyst can be exposed to before losing effectiveness, such as swings in flue gas temperature and sulfur and unburned hydrocarbon concentrations.

Bench-scale and preliminary pilot-scale work was performed in Phase II to address these objectives and the results are discussed in detail in the Phase II final report (Miller, et al., 2000). In the previous testing, pilot-scale tests examined the operation of Engelhard Corporation's NOxCat^{TM}920LT catalyst while firing natural gas. These tests confirmed the observations of the bench-scale tests with simplified (i.e., SO_2 free) flue gas. The objective of the next set of tests, those reported in this section, was to examine the behavior of the catalyst during simultaneous deSO_x-deNO_x operation, wherein a dry sorbent and ammonia were injected into the flue gas.

The overall concept for the low-temperature SCR technology was to reduce NO_x emissions using SCR technology either in conjunction with particulate removal (i.e., simultaneous NO_x control and fly ash removal) or separately from the particulate removal. This would involve either coating the clean side of a ceramic filter with a catalyst or coating ceramic monoliths located on the clean side of a particulate control device (e.g., plenum of a baghouse).

The bench-scale testing was to precede a full-scale demonstration using Penn State's demonstration boiler system with the ceramic filter chamber (described in Section 3.2); however, only pilot-scale testing was performed because the level of industrial interest in this work waned. Engelhard Corporation informed Penn State that a corporate decision had been made not to proceed with catalyzed filter activities. Likewise, Babcock and Wilcox, who had initially expressed interest in this activity because it was complementary to their SO_x-NO_x-Rox-Box^{TM} (SNRB) concept (B&W, 1999), later informed Penn State that the SNRB concept was not a primary business concern. Corning, Inc. was willing to participate in these experiments but with limited involvement so further work with the catalyst at the pilot-scale was conducted. The demonstration-scale tests were not performed however, because of the high cost to coat a large number of ceramic filters or monoliths, while industrial interest for this concept declined.

The pilot-scale testing was performed using Penn State's down-fired combustor (DFC) system. Activities included modifying the DFC system to accommodate ceramic monoliths, performing shakedown testing, and conducting the test program, which are discussed in the following sections.

3.1.1.1 System Modifications and Shakedown

A schematic diagram of the DFC showing the baghouse is given in Figure 3.1.1. The DFC is designed to evaluate the combustion performance and pollutant emissions from various fuels (natural gas, coal, coal-water slurry fuels). The combustor has a 20 inches internal diameter, and is 20 feet high. Each module consists of five 21 inch tall and 20 inch diameter circular refractory sections. A divergent refractory cone, commonly called a quarl, is positioned on top of the four circular refractory sections. The divergent cone top has a half-angle of approximately ten degrees and is fitted with a multi-fuel burner. The combustor is lined with a 3 inch thick refractory material to withstand temperatures up to 1,650 °C. An 8-inch-thick, light weight, high alumina insulation layer was used to minimize heat loss and produce a flame temperature of between 1,450 and 1,500°C. The flue gases pass through a modular heat exchanger that cools them to about 100°C before they exit. Several 4-inch sampling ports are located along the combustor. Sample ports are numbered 1 through 10 starting at the top. Gas samples for compositional analysis were extracted at the exit of the heat exchanger. Wall temperatures are monitored with type-S thermocouples at six locations along the combustor. The

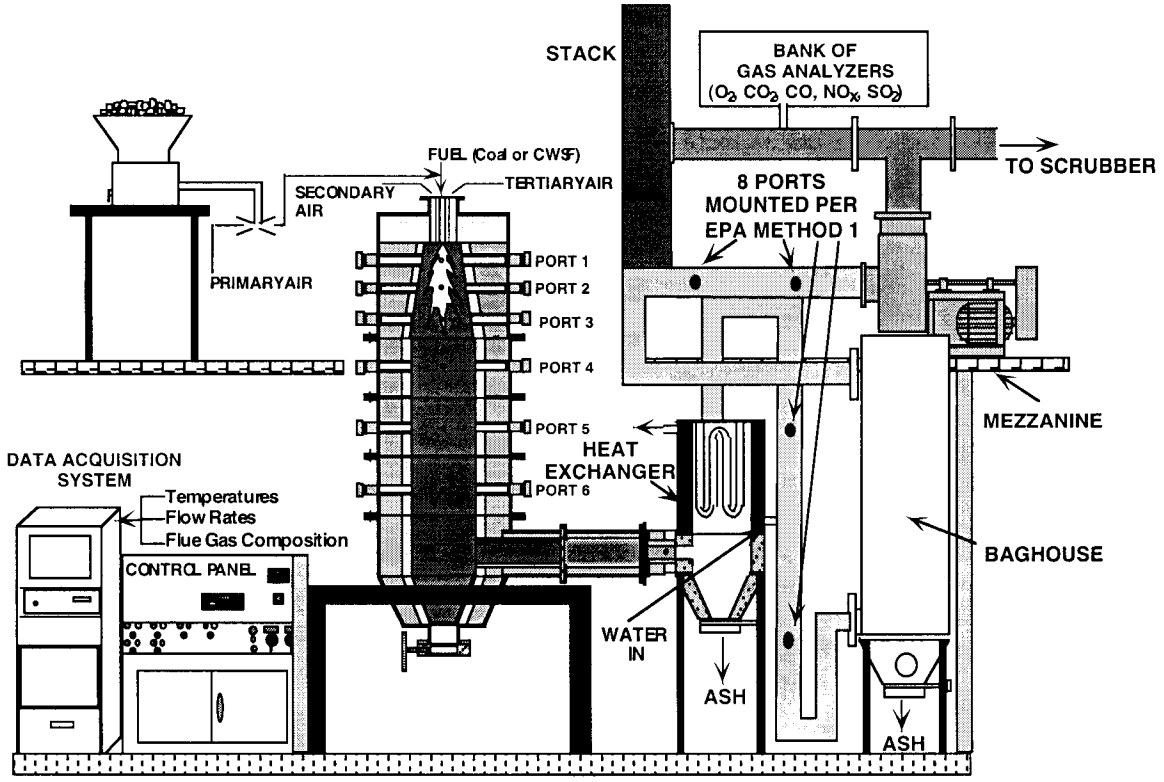

Figure 3.1.1 SCHEMATIC DIAGRAM OF THE 500,000 Btu/h DOWN-FIRED COMBUSTOR AND AUXILIARY COMPONENTS

temperature readings T1 through T6 in the main combustor section are wall temperatures as read by type-S thermocouples. The temperatures of the flue gas entering and leaving the heat exchanger are monitored with type-K thermocouples (T11 and T12). Coal is transported using 10% of the total combustion air through the central pipe. The air that is sent with the coal stream is called primary air. Secondary air is introduced into the annular secondary pipe, which usually constituted 30% of the total air. The balance of the combustion air is introduced as tertiary air. All air streams are introduced at the same height.

In its original configuration, the baghouse contains a 3 by 3 array of cloth bag filters suspended from bag cups on the bottom of a steel tube sheet, with each bag supported internally by a wire cage. Venturis are mounted on the bottom side of the tube sheet, concentric with the bag cups. Blowtubes mounted in the plenum box above the venturis provide a back pulse of compressed air through the filters, thus removing particulate matter from the exterior of the bags.

The modifications to the DFC system included removing the bags and cages from the baghouse, increasing the height of the plenum, relocating the blow pipes, fabricating retaining rings to hold the ceramic monoliths in place, installing sorbent and ammonia injections systems, and installing additional continuous emissions monitors.

Prototype I

Figure 3.1.2 shows the configuration of the baghouse for the first series of tests. In the first round of modifications, the existing tube sheet along with the venturis, bag cups, cages, and bag filters were removed. A new tube sheet (identical to the original) was fabricated and a new set of cages, cups, and filter bags was purchased and installed. The ceramic monoliths were mounted within the bag filters for the first few tests. A platinum catalyzed monolith occupied the central position in the filter matrix while uncatalyzed monoliths were used at the other eight positions. Three-inch diameter Lo-Flo Pitot traverse stations were mounted on top of the tube sheet, above the catalyzed monolith and above one of the uncatalyzed monoliths. Details of the sensors and the traverse stations are provided in the following section (Prototype II), which shows the final configuration of the baghouse modifications. Six inch long flanged extension tubes were mounted above the remaining seven monoliths. The Lo-Flo stations were modified by the addition of 3/8 inch OD ports to permit sampling of flue gas immediately downstream of the monoliths. Venturis were not used in this configuration.

Figure 3.1.3 shows a cross-section of a monolith and its retaining tube. The uncatalyzed monoliths were turned in a lathe in order to reduce their outer diameter to approximately 2 9/16 inches. The platinum-catalyzed monolith was used without modification. The retaining tubes were fabricated from 3 5/16" id, 16-gauge, stainless steel tubing. A flange was welded to the upper end of the retaining tube (the bolt pattern in this flange matched the patterns in the tube sheet and bag cups) and a ring was welded to the bottom of the tube to support the monoliths. The retaining tubes were split in half lengthwise to permit insertion of the monoliths. Two sections of monolith with a total length of 19.2 inches were used in each tube. Pins (2 per monolith) fabricated from 1/16 inch OD welding rod were used to align the hole patterns of the two monolith sections. The monoliths were wrapped in a blanket of Saffil mat insulation and then placed between the two halves of the retaining tube. Stainless steel hose clamps were used to compress the matting, firmly holding the monoliths in place. The retaining tubes and

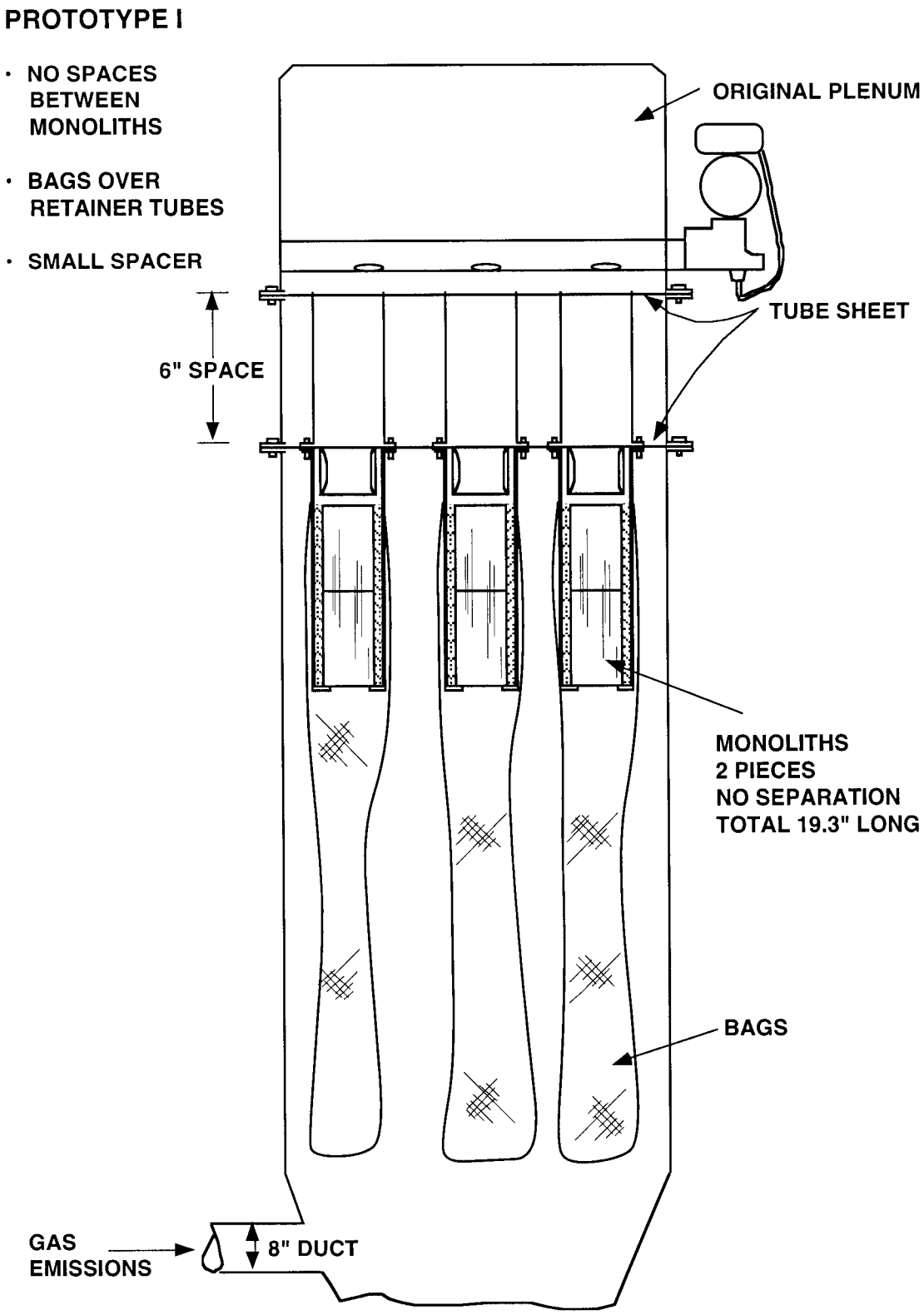

Figure 3.1.2 CROSS SECTION OF BAGHOUSE CONTAINING MONOLITHS IN FILTER BAGS

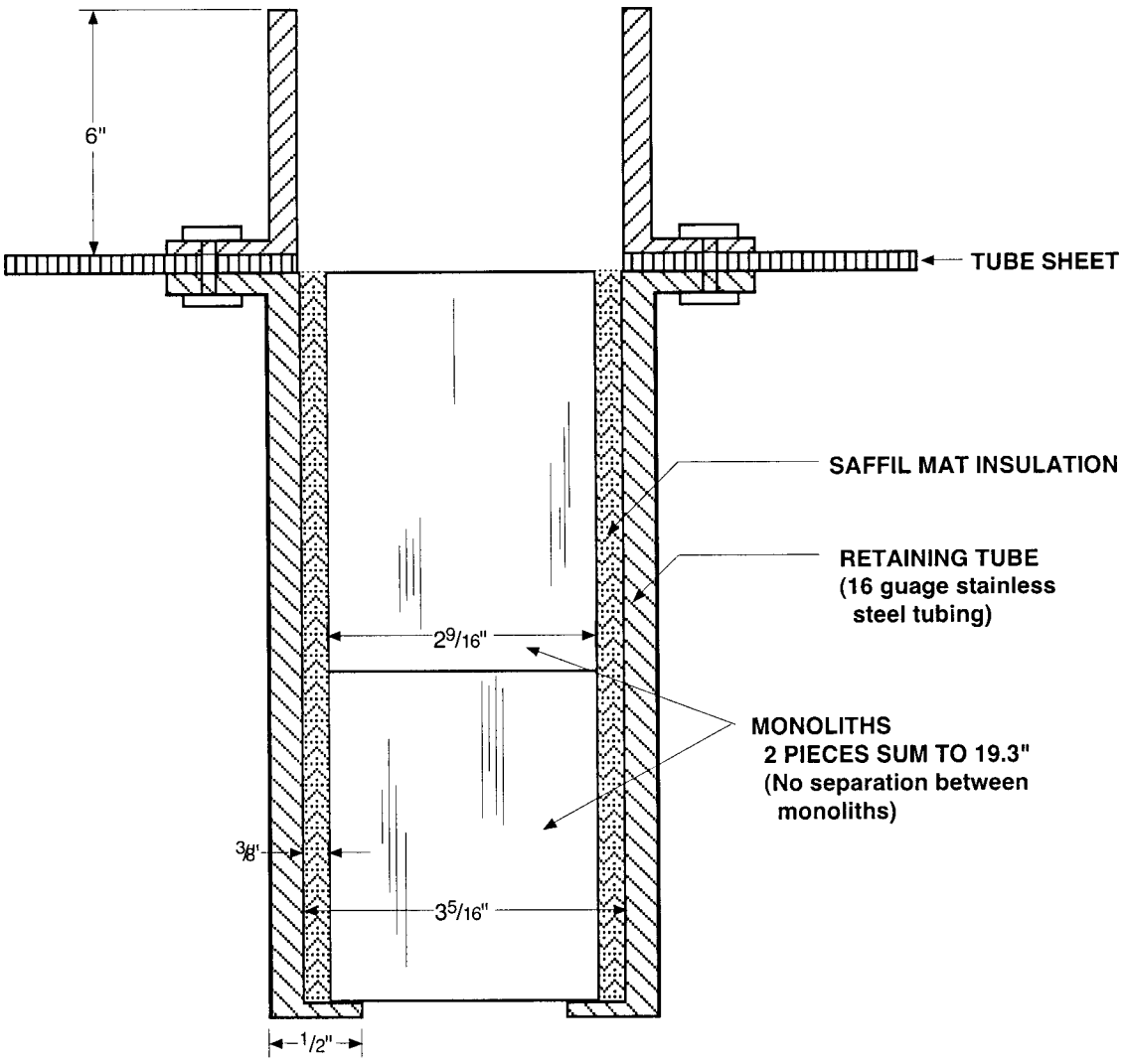

Figure 3.1.3 EXPLODED VIEW OF MONOLITH CHAMBER WITH RETAINING RING

monoliths were then mounted on the bottom side of the tube sheet, concentric with the bag filter mounting cups.

Ports were added to the 8 inch duct between the outlet of the heat exchanger and the inlet of the bag house. The first, located approximately 10 feet upstream of the baghouse inlet was for the injection of sodium bicarbonate into the flue gas stream. The second port, located 5 feet down stream of the sodium bicarbonate injection point, was for the injection of ammonia.

A dry material feeder (Schenck Accurate 102M) was used to inject $NaHCO_3$ into a transport air stream. In order to improve dispersion of the sodium bicarbonate in the flue gas stream, it was injected into the duct against the flow direction. Feed rates could be measured by using a load cell to follow the decreasing mass of the feeder (plus sodium bicarbonate) as a function of time. Initial calibrations of the dry material feeder produced a reliable mapping of feed rate versus control dial setting. However, these tests indicated that the feed rates required for the NO_x reduction study were all compressed in the bottom 10% of the motor speed control potentiometer. The manufacturer of the dry material feeder provided a new feed tube and auger, better suited to the low feed rates required in this study. However, attempts to calibrate the feeder in this configuration proved to be unreliable (repeated measurements of what was ostensibly the same feed rate varied greatly). Thus, all sodium bicarbonate feed rates were measured using the load cell.

Figure 3.1.4 shows the ammonia injection system installed in the 8 inch duct. The flow rate of the ammonia mixture (15% NH_3, balance nitrogen) was measured with a mass flow meter. A nozzle with two outlets was used to inject the ammonia into the flue gas flow. Like the $NaHCO_3$ injection system, the ammonia injector introduced its flow against the flow direction in the duct to improve mixing.

Backpulsing of the baghouse causes a significant increase in the draft pressure in the DFC followed by several seconds of pressure oscillations as the induced draft fan controller recovers from the upset. In order to minimize the impact of baghouse pulsing on the analytical measurements, the portion of the timing circuitry which controls the time between pulses of compressed air was modified. The modified circuit allowed off-times of up to 10 minutes, although typical off-times of approximately 2 minutes (with a pulse duration of 0.5 seconds) were used in this study.

Maintaining the temperature of the monoliths near the values specified in the NO_x reduction test matrix proved to be difficult. Initial tests showed significant heat loss between the inlet and outlet of the baghouse. This problem was alleviated via improvements to the insulation on the exterior of the unit. Regulation of the temperature of the monoliths presented a greater problem. The only temperature control in the baghouse was by varying the flow of water through the heat exchanger. Due to the significant thermal inertia of the system, varying the flow of water usually led to undershooting the desired temperature upon increasing the flow and

overshooting (with the accompanying potential to damage the bag filters) upon decreasing the flow.

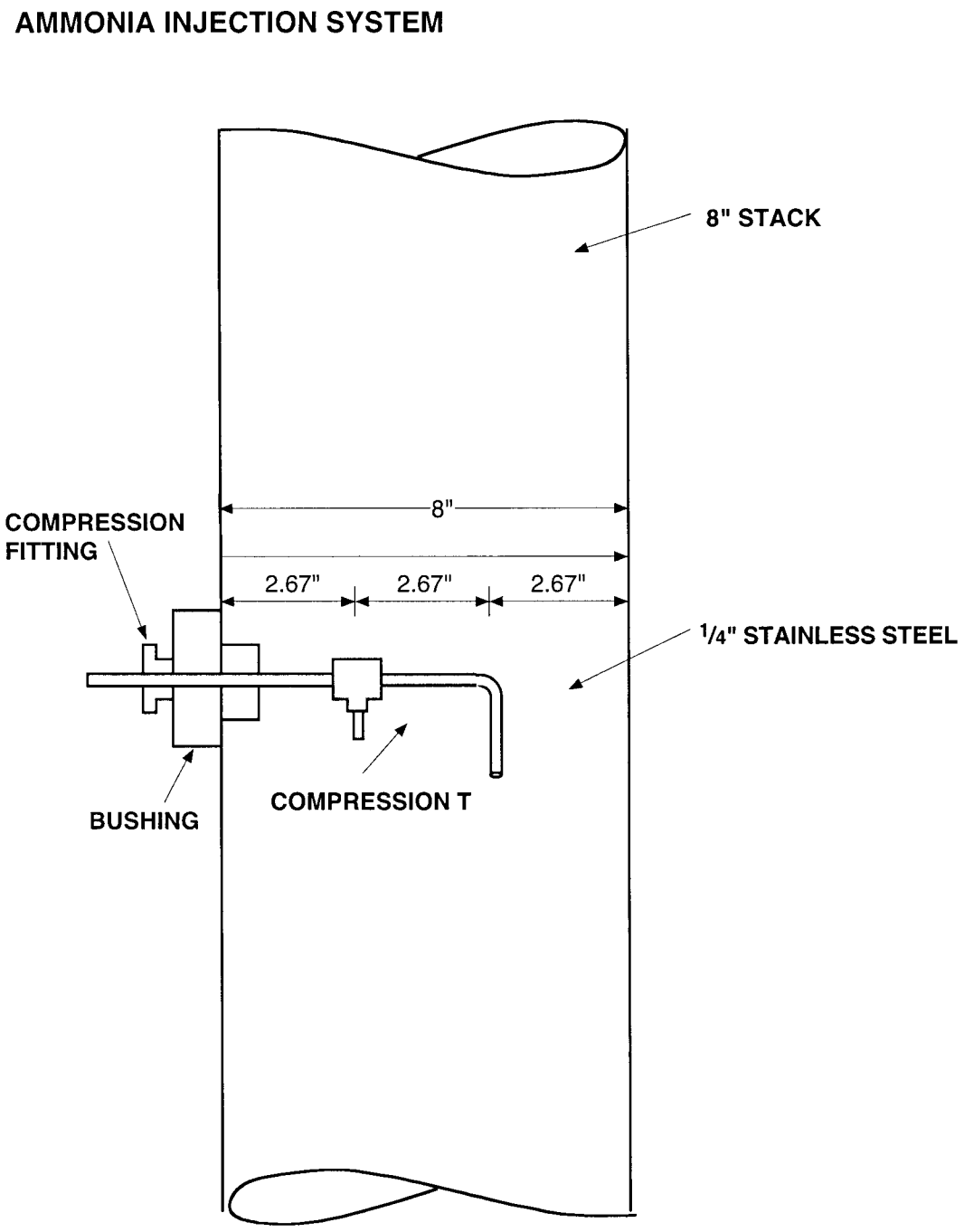

Figure 3.1.4 AMMONIA INJECTION SYSTEM INSTALLED IN 8-INCH INLET DUCT

Initial testing while firing natural gas revealed a large pressure drop (up to 8 inches w.c.) across the baghouse (typically pressure drops of 1 to 2 inches w.c. had been observed in previous studies). Due to this large pressure drop, the induced draft fan was unable to maintain a negative draft pressure even when operating at maximum revolutions per minute. Switching from firing natural gas to firing coal allowed us to decrease the flow of combustion air, thus decreasing the load on the fan. However, this proved to be insufficient and the combustor was shut down due to positive draft pressures and possible leakage of combustion products into the high bay. It was unclear at that time whether this pressure drop was due to clogging of the monoliths or clogging of the bag filters. At the time of these first tests, the only pressure measurement taps were located in the plenum box and in the main body of the baghouse. Thus, only the total pressure drop across the filter bags and monoliths could be measured at this time. A later modification added a pressure measuring tap which permitted the measurement of the pressure drop across the bag filters.

Following the first few days of testing, the unit was disassembled and inspected. The monoliths were found to be relatively clean and it was assumed that the observed pressure drop was due to ineffective cleaning of the bag filters by the compressed air pulse. Venturis were attached to the end of each of the monolith retaining tubes with silicone adhesive. Caked-on ash was removed from the exterior of the bag filters and the system was reassembled. A test firing of the system on natural gas revealed similar results. The pressure drop across the system increased with time presumably due to inefficient removal of ash from the exterior of the bag filters.

Modifications were made in an attempt to improve the effectiveness of the baghouse pulsing system (see Figure 3.1.5). The original tube sheet, bag cups, and venturis, along with the bag filters used in the series of tests described above, were installed in the baghouse. A 30-inch high galvanized steel spacer (see Figure 3.1.6) with blowdown tubes was fabricated and installed on top of this tube sheet. Then the tube sheet used for the previous series of tests (along with the monoliths and retaining tubes, low-flow stations, and extension tubes) was installed on top of the spacer. Finally, the 6-inch spacer from the previous tests and the plenum box were installed on top of this assembly.

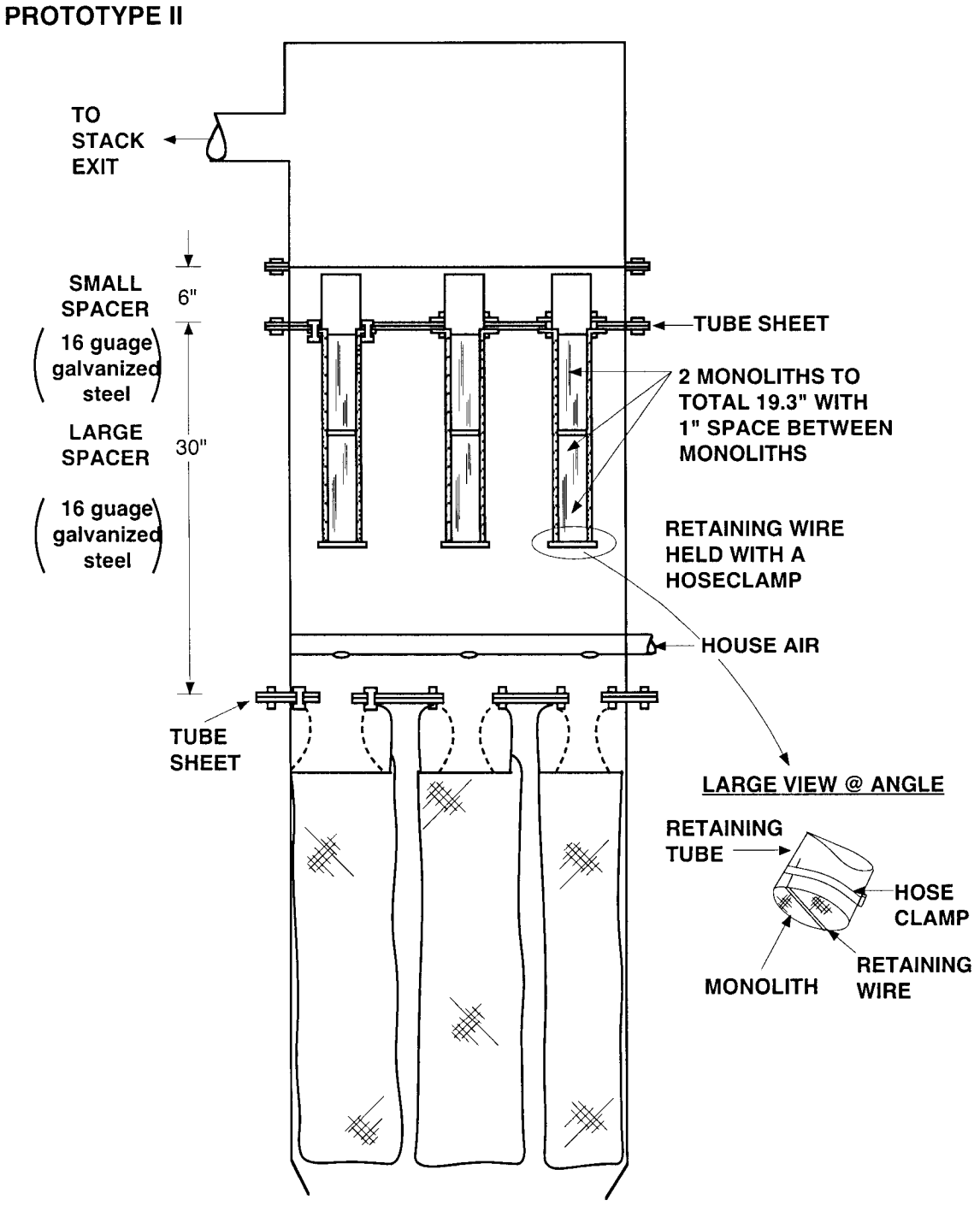

Figure 3.1.5 CROSS SECTION OF BAGHOUSE WITH MONOLITHS ABOVE FILTER BAGS

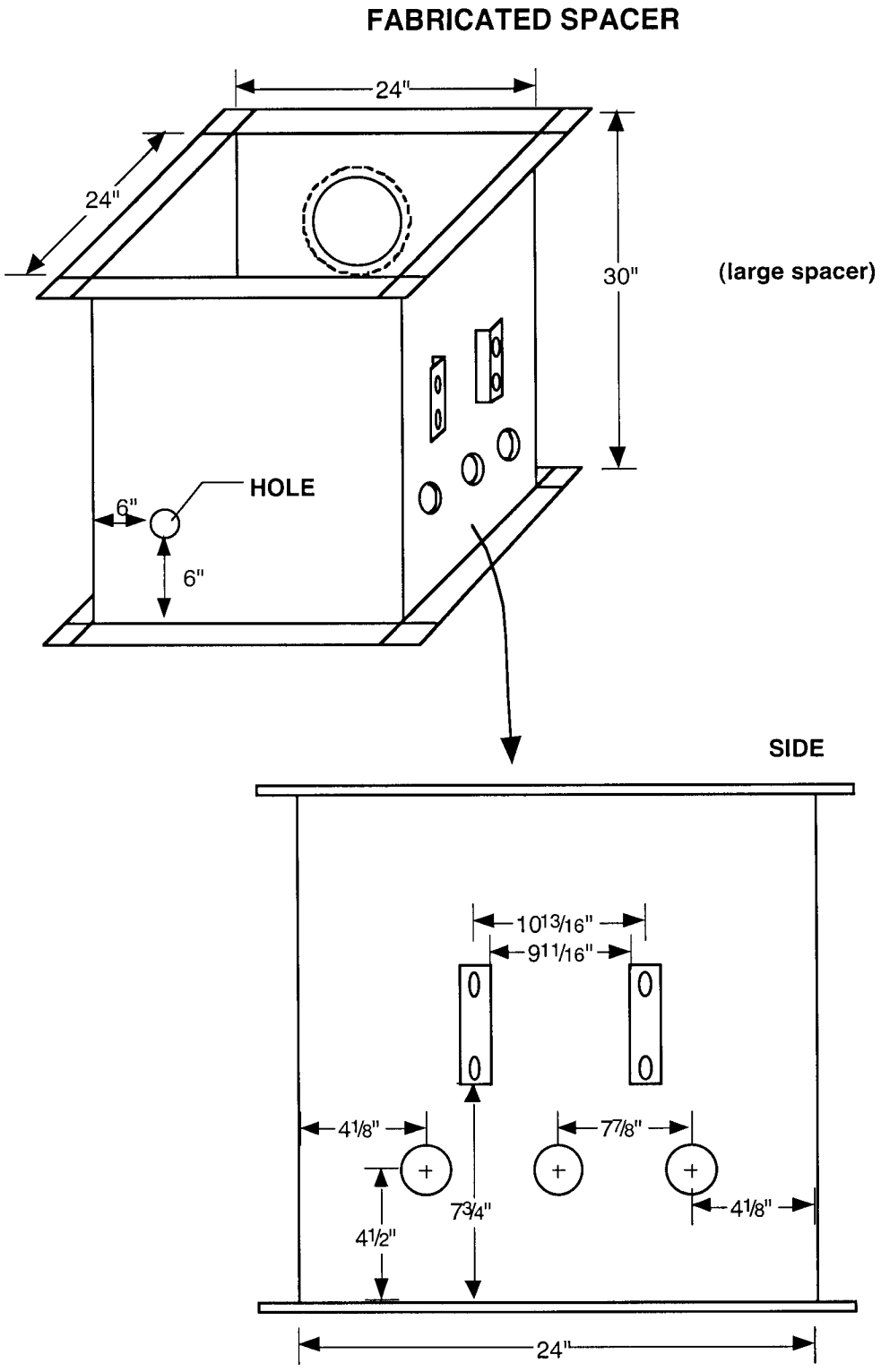

Figure 3.1.6 30-INCH SPACER USED IN HOLDING MONOLITHS

An additional step was taken to mitigate the pressure drop problem by increasing the capacity of the induced draft fan. A larger motor (15 HP versus 10 HP) and a new inverter sized for the 15 HP motor were installed. In addition, the rotational speed of the fan was increased by changing the pulleys on the shaft of the motor and the shaft of the fan.

Following subsequent testing, ash build up was found in the plenum box region. The system was torn down and holes were found in the bag filters. Apparently these filters were damaged while inserting the tube sheet/bag filter assembly into the baghouse. The filters were replaced with a used set of bags, which were removed prior to the NO_x reduction testing.

Throughout most of these early tests, reliable readings were not obtainable from the low-flow Pitot stations. The readings were frequently zero or fluctuated wildly (between reasonable values, based upon the experimental conditions, and zero). Apparently, the flows were near the minimum flow threshold required to produce a stable reading on these flow stations. The tubing and fittings between the flow stations and the transmitter (including all connections within the plenum box) were checked for leaks and none were found.

Prototype II

The modifications to the baghouse for the second prototype centered around the flow stations. Two airflow stations were installed to measure the flow and space velocities through two of the nine ceramic monoliths, as shown in Figure 3.1.7. The low-flow stations, fabricated of type 316 stainless steel pipe and a Veltron II transmitter, were purchased from Air Monitor Corporation. The low-flow stations provide highly accurate measurement of low air volumes for monitoring, controlling, and indicating applications when connected to the Veltron II transmitter.

One of the flow stations was mounted on the pipe containing the catalyzed monolith while the other one was mounted on one of the eight remaining uncatalyzed monoliths. Three stainless steel tubes were connected to each flow station. One tube was used to withdraw a flue gas sample. The other two tubes were used to read static and total pressures. Each of the two tubes were plumbed into an inline three-way valve and then into the Veltron transmitter where the flow is read in ACFM. The 3/8-inch three-way valves were used to switch between the catalyzed and uncatalyzed monoliths, as the transmitter was equipped to read only one flow station at a time.

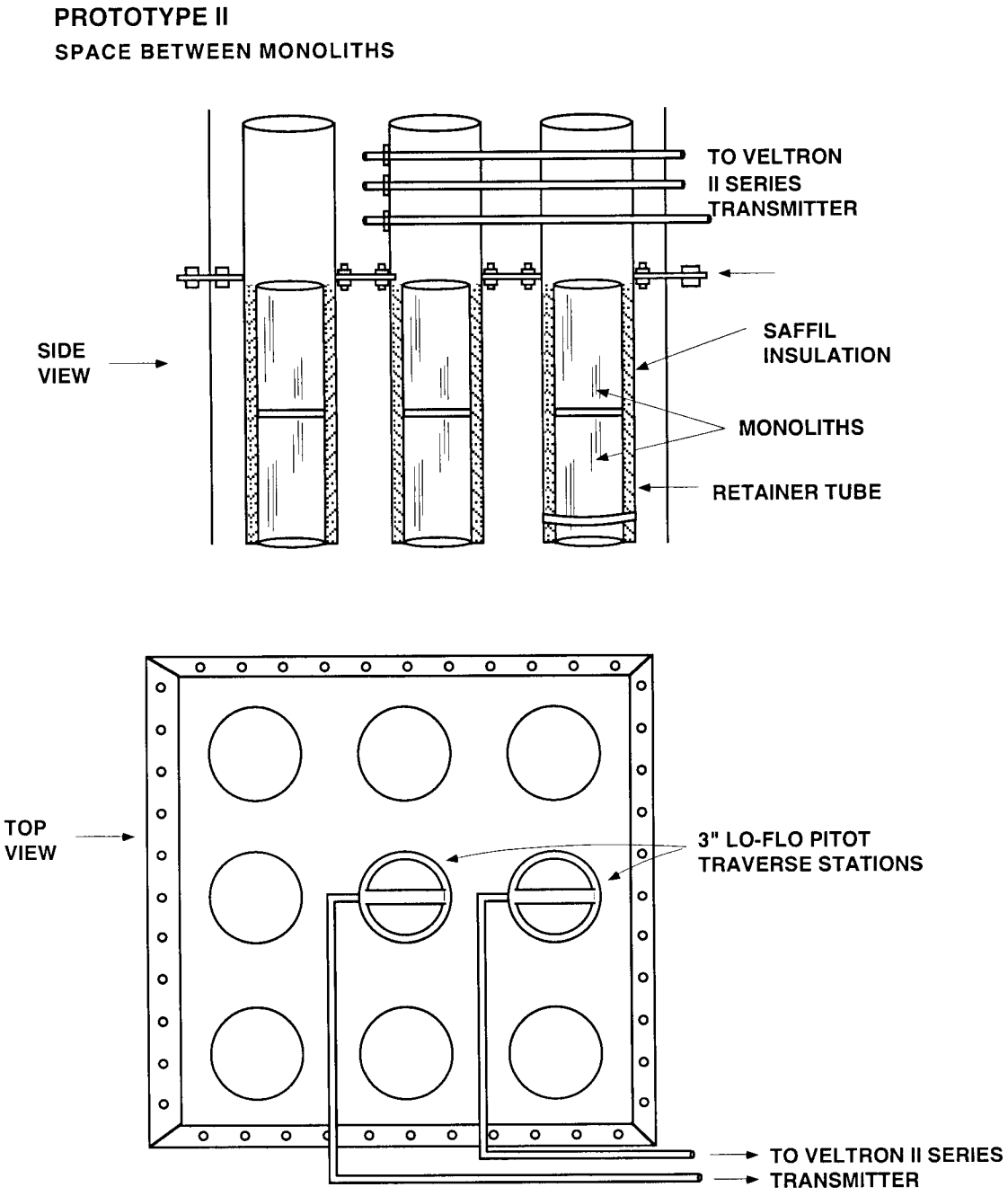

Figure 3.1.7 SIDE AND TOP VIEW WITH LO-FLO STATIONS AND TUBING

Several problems were encountered when testing resumed. The transmitter did not record a reading for the catalyzed monolith and varied between zero and 14 actual cubic feet per minute (ACFM). After several tests, it was determined that the detection limit for the transmitter was 14 ACFM and would not yield any value below this limit. It was also determined that the

catalyzed monolith presented a higher resistance to flow than the uncatalyzed monolith. The solution was to cap four of the eight uncatalyzed monoliths in order to increase the flow through the remaining monoliths. Four brass pipe fittings were secured in place using Dow Corning RTV sealant 736, a sealant resistant to heat up to 500°F. The monoliths on each corner were capped to maintain a symmetric flow regime through the remaining monoliths.

The next test yielded better results in that the flow station had sufficient flow and attainable transmitter readings. As the monolith temperature steadily rose from 100°F to approximately 375°F, the flow through each of the two monoliths increased steadily from 31 to 38 ACFM for the uncatalyzed monoliths and from 15 to 24 ACFM for the catalyzed monoliths. This test confirmed that the lower detection limit for the transmitter was approximately 14 ACFM.

The parameters chosen for the testing included space velocities on the order of 12,000hr^{-1}. At a space velocity of 12,000 hr^{-1}, the flow through the five monoliths that were left uncapped was too high. Appropriate flow through each monolith should be approximately 16 ACFM. It was decided to uncap two of the four monoliths before the next set of tests. To maintain a symmetric flow regime, two monoliths on opposite corners were uncapped while the remaining two were left capped. After several more tests, there was inconsistency in maintaining the desired flow through the seven open monoliths. Problems with flow rates were also encountered when sodium bicarbonate was fed via an airswept system into the 8-inch duct before entering the baghouse (see Figure 3.1.4). Slide gates were then added to two of the monoliths thus allowing manual control of the flow. Because of the tight arrangement, only two of the monoliths were fitted with slide gates. The slide gates were installed on monoliths located at opposite corners and could be manually manipulated by handles located outside the plenum box. The final arrangement contained seven uncapped monoliths, two of which could be left open or closed.

Several other modifications were also made at this time. Three-inch collars made from aluminum flashing were attached to the top of the low-flow stations. This extended the length of the flow stations and helped to alleviate the flow from mixing back down into the top of the stations, which could result in a false reading or noise in the transmitter reading. The insulation on the two spacers and plenum box was greatly improved at this time.

Several more tests were conducted with these modifications. More problems existed with the flow through the catalyzed monolith. The transmitter indicated a value of zero for most of

the testing and indicated an average of 28 ACFM for the uncatalyzed monoliths. The pressure drop across the bags gradually increased with the addition of each new test. The pressure drop increased from approximately 1 to 3 inches w.c. to 8 to 9 inches w.c. This led to a visual inspection of the filter bags, which had been damaged.

The filter bags were replaced with new P84 felt filter bags and were properly seeded with crushed limestone per the manufacturer's instructions. After installation, the average pressure drop was 2.4 inches w.c., which was expected for typical operation.

The monolith configuration was changed per a conversation with a representative from Englehard, who coated the monoliths with the catalyst. The testing to this point consisted of two monolith sections stacked atop one another to accommodate a length of 19.3 inches and were supported with a pipe and retaining ring as shown in Figure 3.1.3. It was recommended by Englehard that there be at least a one-inch space between each section of monolith if they are to be stacked. To allow for this spacing, the retaining ring was removed from the bottom of the pipe. Two monolith sections, with a one-inch space, were held in place with the pressure exerted from the retaining pipe and Saffil insulation. A small piece of rigid wire was used for added support at the bottom of the pipe. The wire was molded around the bottom of the pipe and held in place with a hose clamp as can be seen in Figure 3.1.8. Lastly, to assure the monoliths were not contaminated, an eight-inch section was returned to Engelhard Corporation for evaluation and determined to be worthy for use.

3.1.1.2 Preliminary Testing and Results

Preliminary low-temperature SCR testing was performed and included experiments to establish the range of test parameters such as flue gas temperature, space velocity, and to shake down the $NaHCO_3$ and NH_3 injection systems. A test matrix was developed based on the preliminary testing where the flue gas flow rate through the monoliths (i.e., space velocity) and temperature limitations of the fabric bags were determined. The test matrix is given Table 3.1.1

The commercially available platinum-based NOxCat LT 920 catalyst used in this study was supplied by the Engelhard Corporation. It contained 200 cells per square inch (cpsi). Testing performed in an earlier evaluation of the SCR process at higher temperatures utilized the same catalyzed monoliths. To eliminate concern over its continued reactivity, a sample of the catalyzed monolith was returned to Engelhard Corporation for evaluation. This evaluation was

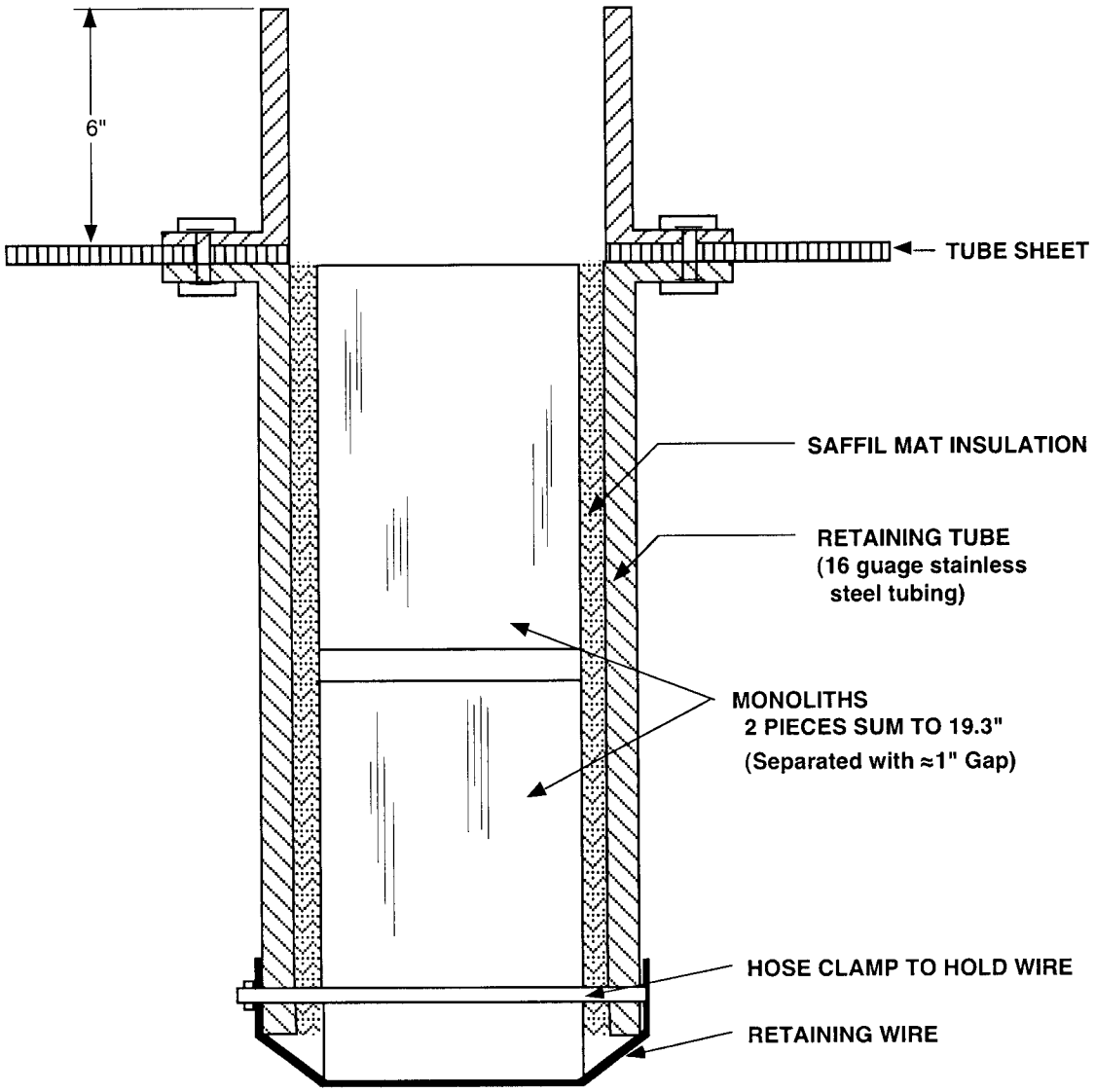

Figure 3.1.8 EXPLODED VIEW OF MONOLITH CHAMBER WITH RETAINING WIRE

performed at 392 and 482°F and space velocities of 20,000 and 60,000 hr^{-1} using a synthetic flue gas containing 10% oxygen, 10% water, and 500 ppm NO and NH_3. The evaluation conducted at 392°F reported 17.7 and 7.8% conversions of NO at space velocities of 20,000 and 60,000 hr^{-1}, respectively. These results indicate 5% lower conversions than reported in the Phase II final report for a catalyst containing only 100 cpsi tested under similar conditions (Miller et al., 2000).

Table 3.1.1 Low-Temperature SCR Test Matrix

Test Number	Space Velocity (hr^{-1})	Flue Gas Temperature (^oF)	NH_3/NO Molar Ratio
1 - 4	12,000	325	0.6, 0.8, 1.0, 1.2
5 - 8	12,000	375	0.6, 0.8, 1.0, 1.2
9 - 12	12,000	425	0.6, 0.8, 1.0, 1.2
13 - 16	24,000	325	0.6, 0.8, 1.0, 1.2
17 - 20	24,000	375	0.6, 0.8, 1.0, 1.2
21 - 24	24,000	425	0.6, 0.8, 1.0, 1.2
25 - 28	48,000	325	0.6, 0.8, 1.0, 1.2
29 - 32	48,000	375	0.6, 0.8, 1.0, 1.2
33 - 36	48,000	425	0.6, 0.8, 1.0, 1.2

Possible poisoning or fouling of some catalytic sites may have occurred in the earlier testing of this catalyst. At a higher temperature of 482°F, 53 and 37% conversions were measured for 20,000 and 60,000 hr^{-1}, respectively. The evaluation also indicated that greater than 50% of the NO was converted to N_2O, yielding a low selectivity.

The testing in this subtask was to examine the simultaneous deSOx-deNOx operation by injecting ammonia and dry sodium bicarbonate into the duct upstream of the DFC baghouse. Initial tests to examine the use of dry $NaHCO_3$ injection for the removal of SO_2 were performed while maintaining an average baghouse inlet temperature of 500°F. The goal was to demonstrate 90% SO_2 reduction at the baghouse outlet. Reducing the SO_2/SO_3 concentrations to very low levels minimizes the formation of ammonium bisulfate (ABS) during SCR operation. The deposition of ABS results in fouling of the catalyst surface. Earlier testing injecting sodium bicarbonate in the demonstration boiler system had shown greater than 90% reduction in SO_2 emissions at a Na_2/S molar ratio of 1.65. A time interval of 1.5 minutes between backpulses for cleaning the bags was used for this testing. A greater time interval was not possible with the backpulse controls. The timer for backpulsing of the DFC baghouse has been modified to allow up to 10 minutes between backpulses. This should allow greater control in optimizing the feed rate of $NaHCO_3$ and its retention on the filter bags. Initial testing of this system indicated that greater than 90% reduction of the SO_2 was achievable at lower Na_2/S molar ratios in the DFC system.

The preliminary testing with NH_3 injection provided results that compared well with those provided by Engelhard Corporation. Consequently, the test program listed in Table 3.1.1 was performed.

3.1.1.3 Low-Temperature SCR Testing and Results

Pilot-scale testing was performed to evaluate the use of the low temperature selective SCR catalyst with NH_3 injection for the control of NO_x emissions from a coal-fired industrial boiler. As previously mentioned, this testing utilized an approach similar to the SO_x-NO_x-Rox-Box™ technology. The objective of this testing was to evaluate the modified SNRB approach for controlling NO_x emissions at conventional baghouse temperatures, typical of those observed in the flue gas from an industrial boiler. The goal of this phase of testing was to evaluate this technology for simultaneous control of SO_2, NO_x and particulate emissions while burning coal in the DFC to determine if bench-scale results could be matched, in which significant conversion of NO was obtained at a catalyst temperature as low as 480°F (Miller et al., 2000).

SO_2 Emissions Control

Control of the SO_2/SO_3 emissions was accomplished through the injection of a dry sorbent, sodium bicarbonate ($NaHCO_3$), upstream of the fabric filter. Church and Dwight supplied the sorbent grade–extra fine sodium bicarbonate used in this study. The bicarbonate had a particle size distribution of greater than 95% passing 200 mesh and a mass median diameter of 35 μm. Sodium bicarbonate was chosen as the sorbent since it endothermically decomposes at relatively low temperatures, 250°F and above, forming a surface of sodium carbonate to react with acidic gases such as SO_2. This decomposition proceeds by the following reaction:

$$2NaHCO_3 \rightarrow Na_2CO_3 + CO_2 + H_2O$$

Several factors including flue gas temperature, humidity, and concentration of CO_2 affect the rate of decomposition. Although the flue gas velocity and the location of the injection site provided little residence time before the entrance to the fabric filter, evaluations of dry sorbent injection have shown high percentages of decomposition with less than 1 second at temperatures as low as

275°F (EPRI, 1990). After decomposition, the sodium carbonate reacts with SO_2 by the following reactions:

$$Na_2CO_3 + SO_2 \rightarrow Na_2SO_3 + CO_2$$

and

$$Na_2CO_3 + SO_2 + 1/2\ O_2 \rightarrow Na_2SO_4 + CO_2$$

The purpose of sodium bicarbonate injection was not to perform a detailed investigation of the sorbent's performance in capturing sulfur. This examination was performed in Phase II of the project (Miller et al., 2000). Instead, the goal of the dry sorbent injection was to reduce the concentrations of SO_2 and SO_3 in the flue gas, thus preventing the possible formation of ammonium bisulfate, $(NH_4)_2SO_2$ or NH_4HSO_4. When sulfur is present in the flue gas, a small percentage of the SO_2 formed undergoes further oxidation to SO_3. The SO_3 can react with H_2O to form sulfuric acid, which can then combine with NH_3, resulting in the formation of ammonium bisulfate (ABS). The ABS, at temperatures typical of those inside a fabric filter (300 – 450°F), can deposit on and foul downstream equipment including the SCR catalyst. Therefore, it is important to remove as much of the SO_2 and SO_3 as possible from the gas stream. The goal for SO_2 removal was a minimum of 90%.

NO_x Emissions Control

SCR is a widely accepted technology for the control of NO_x emissions from fossil fuel combustion. The most commonly applied type of catalyst is a monolith coated with vanadia-titania. This type of catalyst displays a high reactivity at temperatures between 500-800°F. However, at the lower temperatures (338-482°F), typical of the flue gas leaving an industrial boiler, the reactivity drops off considerably. As a result, platinum, which has a higher reactivity at lower temperatures, becomes the active catalytic component of choice.

For the testing, a Middle Kittanning seam coal was burned and ammonia was injected for the NO_x control. Upon contacting the catalyst, the NO reacts with the ammonia by the following desired reactions:

$$4NH_3 + 4NO + O_2 \rightarrow 4N_2 + 6H_2O$$

and

$$4NH_3 + 2NO_2 + O_2 \rightarrow 3N_2 + 6H_2O$$

Particulate Emissions Control

A commercially-available baghouse was used for removing the particulate matter from the flue gas. Nine teflon coated fiberglass felted bags removed the fly ash and dry sorbent prior to the flue gas contacting the SCR catalyst. This type of fabric has a maximum temperature rating of 500°F, typical for most boiler applications. The test conditions were chosen to eliminate the need for high-temperature filter bags, which are significantly more expensive than convential filter bags. Also, consideration was not given to the use of flue gas reheating since this option would certainly decrease the overall system efficiency.

Backpulsing of the baghouse determines the exposure time of the sodium bicarbonate to the flue gas while retained on the filter bags. In order to increase the exposure time and minimize the impact of baghouse pulsing on the analytical instrumentation, modifications were made to the timing circuit board. These modifications allowed up to 10 minutes in off-times, although typical off-times of 1.75 minutes were used in this study. No attempt was made to optimize these operating conditions for greater sorbent utilization.

The particulate dust loading present in the baghouse outlet was not measured during this evaluation. However, it is assumed that a typical collection efficiency for this type of fabric, approximately 99.2%, was observed. Occasional inspections of the baghouse plenum and the ceramic monoliths indicated only small amounts of ash penetration. Therefore, blinding of the active catalytic sites with fly ash was not expected

Experimental

The DFC was preheated on natural gas until the wall temperature inside the divergent cone on top of the combustor reached approximately 1,800°F. The coal was then progressively introduced and the natural gas decreased until the combustor was firing only coal. An average firing rate of 350,000 Btu/h was used for most of the testing. The firing rate, combined with separate control of the inlet cooling water to the heat exchanger, provided the desired flue gas temperatures entering the baghouse. A cross section of the baghouse showing the location of the monoliths is given in Figure 3.1.9. Care was exercised not to exceed the maximum temperature rating of the filter bags.

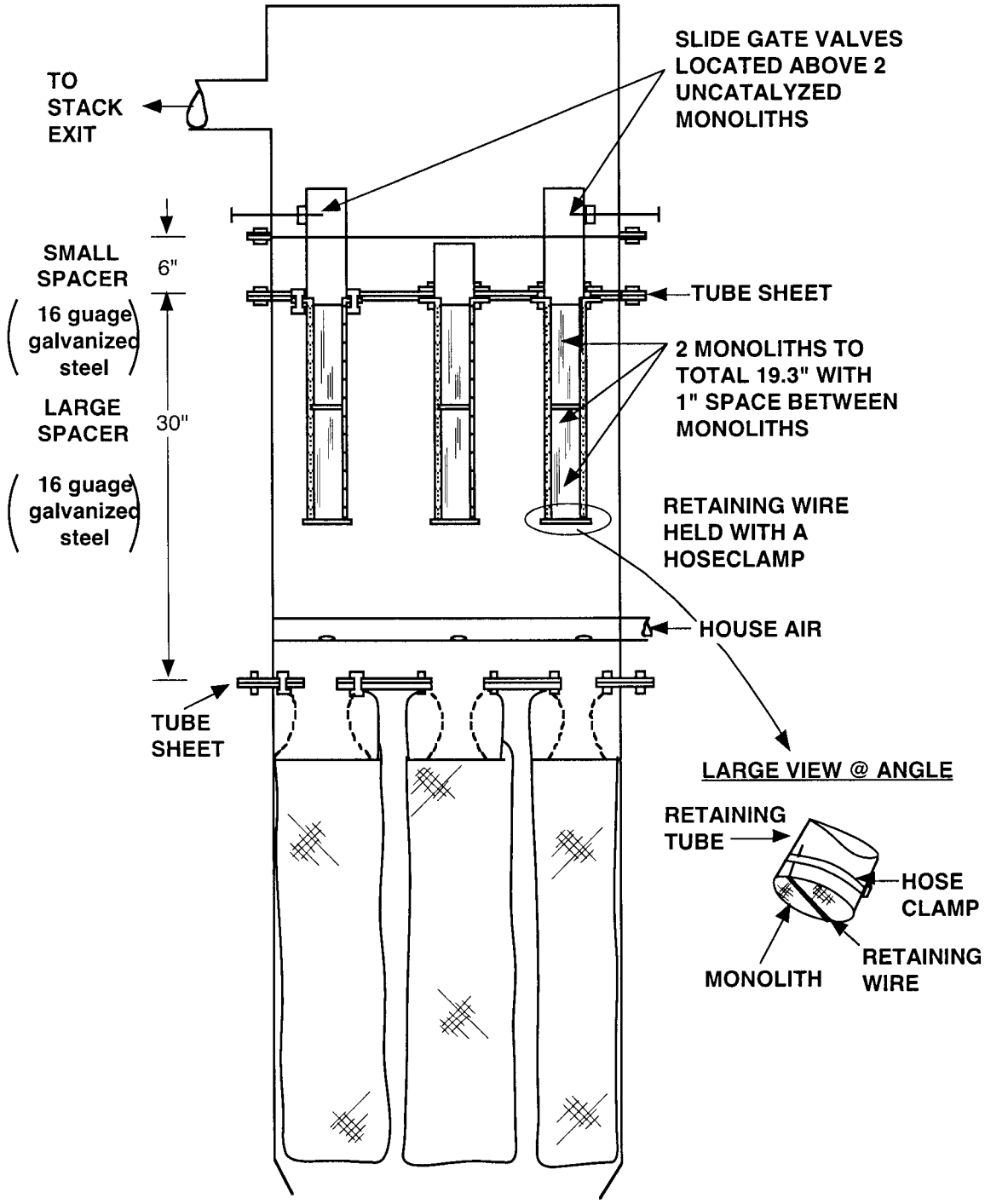

Figure 3.1.9 CROSS SECTION OF BAGHOUSE WITH MONOLITHS ABOVE FILTER BAGS

A Middle Kittanning seam coal was burned for all tests performed in this evaluation. A typical composition of the coal is given in Table 3.1.2.

Table 3.1.2 Typical Composition of the Middle Kittanning Seam Coal

Proximate Analysis, (wt.%, dry)	
Volatile Matter	31.0
Ash	4.5
Fixed Carbon	64.5
Ultimate Analysis, (wt.%, dry)	
Carbon	81.9
Hydrogen	5.1
Nitrogen	1.6
Sulfur	0.7
Oxygen	6.3
Ash	4.5
Higher Heating Value, Btu/lb	14,050

The following flue gas composition was produced at the combustor exit (dry basis) when the Middle Kittanning seam coal was burned in the DFC at an excess air level of approximately 20%:

Oxygen	3.5 – 4.5 %
Carbon Monoxide	75 – 150 ppm
Carbon Dioxide	14.5 – 15.5 %
Sulfur Dioxide	400 – 475 ppm
Nitrogen Oxides	650 – 750 ppm

After achieving stable operation on coal, dry sorbent injection was started and the rate adjusted to obtain 90% SO_2 reduction.

Prior to injecting ammonia, the flow rate through the catalyzed monolith was measured using a lo-flo traverse station mounted above the monolith retainer tube. The flow rate was then adjusted to achieve the desired space velocity by opening or closing the slide gate valves over the uncatalyzed monoliths. Side and top views of the ceramic monoliths are shown in Figure 3.1.10.

The ammonia was supplied from compressed gas cylinders containing 15 vol% NH_3 and a balance of nitrogen. A manual valve was used to adjust the flow rate, and it was measured by a series 8000 thermal mass flow meter manufactured by Eldridge Products, Inc. The required

injection rate of ammonia was determined from the desired NH_3/NO molar ratio, the volumetric flue gas flow rate, and the NO_x concentration in the flue gas entering the baghouse. This system, once adjusted, provided a stable flow rate of injected ammonia into the system.

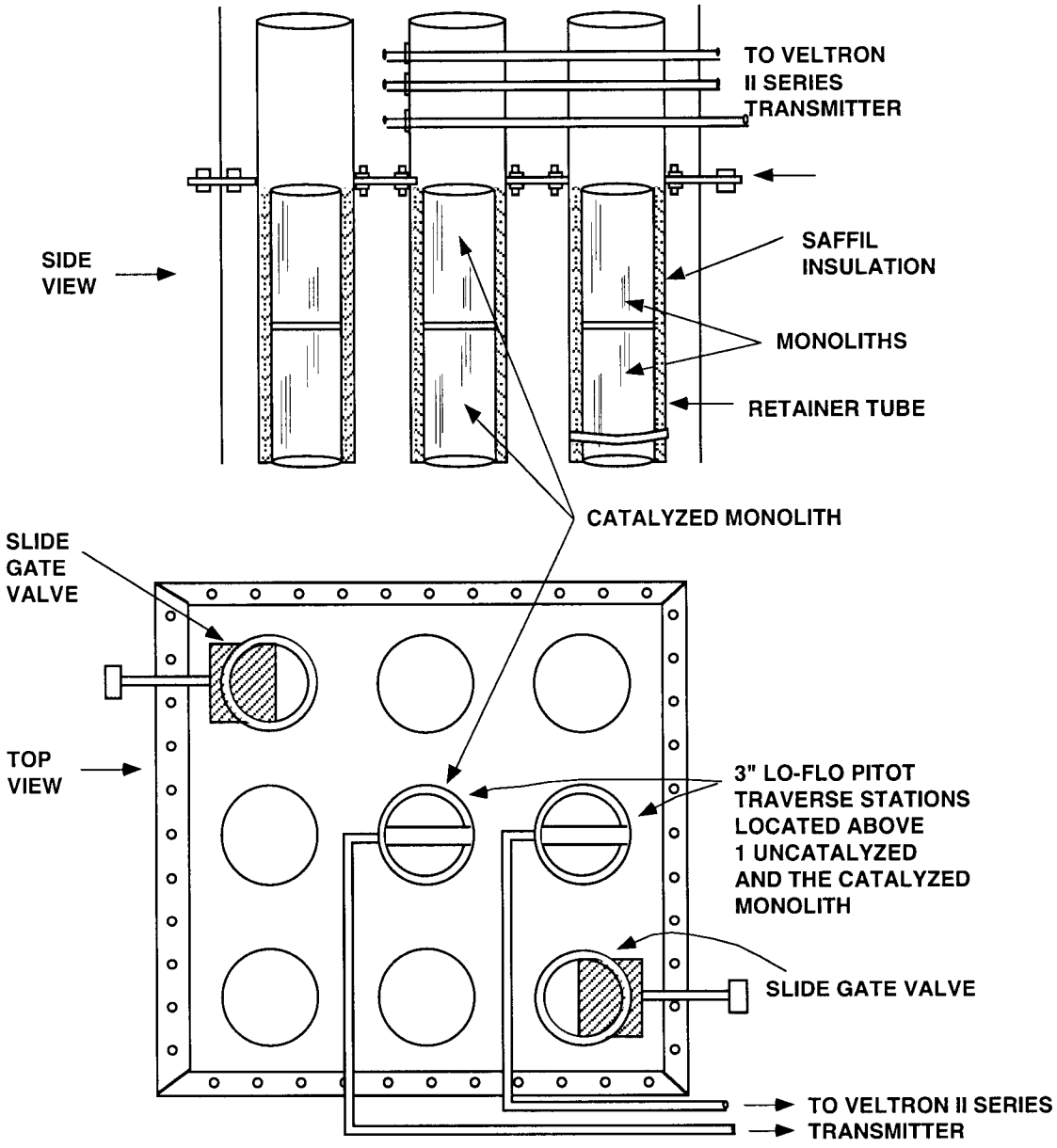

Figure 3.1.10 SIDE AND TOP VIEW WITH LO-FLO STATIONS AND TUBING

Data collection was initiated once the desired test conditions were reached. Two emissions monitoring systems (CEMS) measured O_2, CO, CO_2, SO_2, and NO_x concentrations

prior to the dry sorbent injection location and at the baghouse outlet. The chemiluminescent NO_x analyzers have the ability to measure the NO and NO_2 separately. This allows for the determination of the fate of NO during the injection of the sodium bicarbonate or ammonia. N_2O and NH_3 analyzers were added to the baghouse outlet to measure the catalyst selectivity and NH_3 slip.

Results

Sulfur Capture

Initial shakedown tests injecting sodium bicarbonate at varying rates upstream of the fabric filter were performed to determine the minimum injection rate required to yield 90% reduction in the SO_2 concentration. The results of these tests are plotted in Figure 3.1.11. An average normalized stoichiometric ratio (NSR) of 2.5 was required to achieve an SO_2 reduction of greater than 90% at the conditions tested. The average percent SO_2 reduction at a given injection rate was lower than that achieved by other researchers and during earlier tests evaluating this process on the demonstration boiler facility (Miller et al., 2000), probably because the system was not optimized.

Sodium Utilization

Sodium utilization calculated for these tests ranged between 25-47%. This indicates a very low level of effectiveness when compared to typical sodium utilizations of 70%. Previous evaluations have shown a direct correlation between increasing the flow rate or air-to-cloth ratio (A/C) and increasing sodium utilization (EPRI, 1990).

An examination of the fabric filter specifications indicated that it was designed for an air-to-cloth ratio of 4.2:1 at a flue gas volume of 275 ACFM. An average flue gas volumetric flow rate of 200 ACFM and an A/C ratio of 3.0:1 were used in this study to maintain an acceptable catalyst space velocity. This lowering of the A/C ratio may account for approximately a 5 – 10% decrease in the sodium utilization. However, sorbent particle fallout in the duct and fabric filter hopper are more likely to be the cause of the lower level of SO_2 removal and poor sodium utilization.

Typical duct velocities for an industrial coal-fired system are between 30 – 60 feet/second. Due to the large diameter ducts used on the down-fired combustor, flue gas

velocities of less than 10 feet/second are common with a flue gas volumetric flow rate of 200 ACFM. This low duct velocity results in sorbent fallout in the duct and in the hopper, where lower temperatures inhibit decomposition and where contact with, and capture of SO_2 are severely diminished.

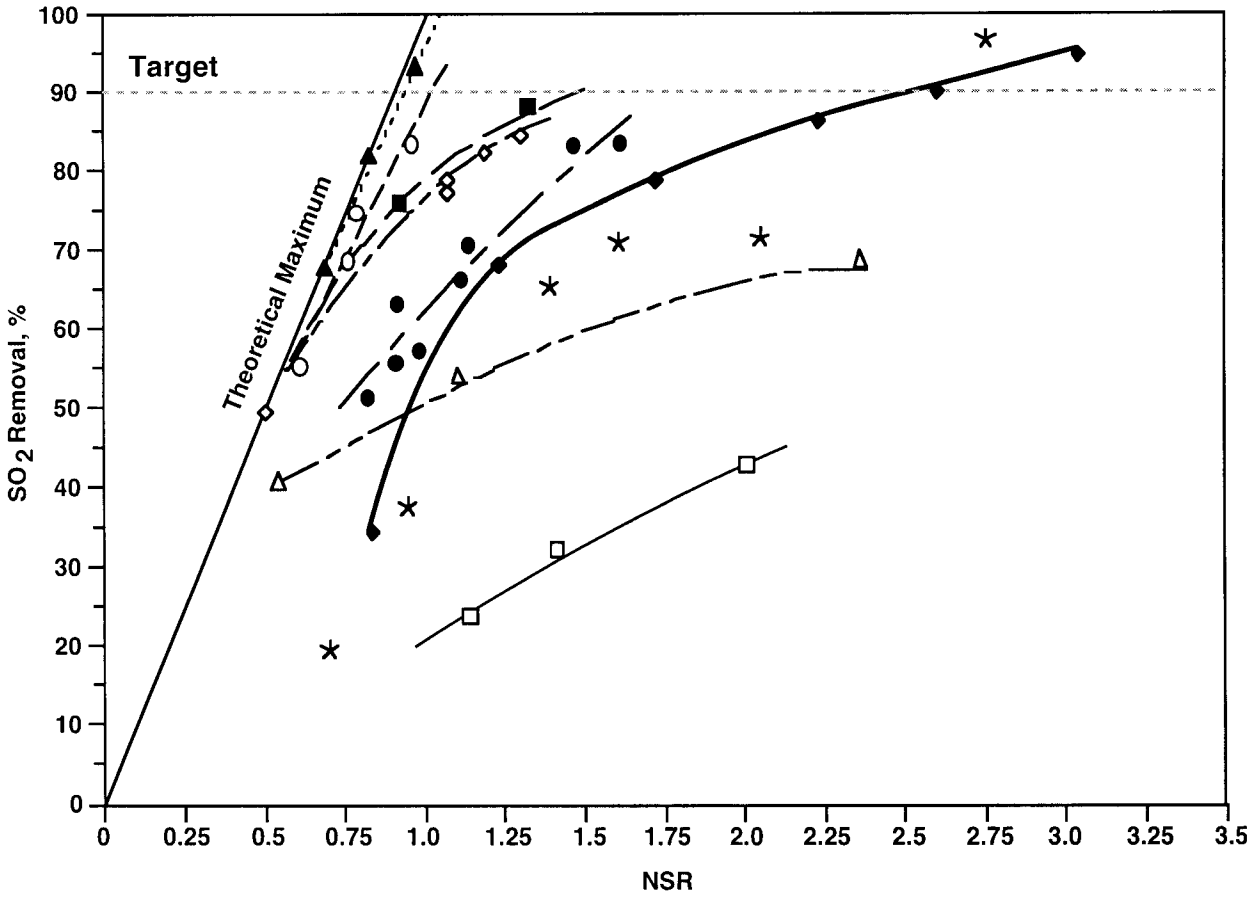

I.D. Code	MMD, μm	Symbol
BA7	9	▲
BA6	9	○
BA5	27	■
BA2	32	◇
BA1	46	●
BA3	75	△
BA4	89	□
PSU-Demonstration Boiler	35	◆
PSU-DFC	35	✶

3.1.11 COMPARISON OF SO_2 REMOVAL AS A FUNCTION OF NSR AND PARTICLE SIZE PSU Flue gas temperature: (Demonstration Boiler ~380°F; DFC ~425°F) - All others tested at ~300°F

An additional reason that lower sodium utilizations were experienced is a shorter residence time for sorbent retention in the form of filter cake on the bags. During testing, an interval of 105 seconds between pulses was used in cleaning the fabric filter. No attempt was made to optimize the utilization by lengthening the delay between pulses, thus extending the sorbent's exposure to the flue gas. Previous testing indicated that a decrease in the NSR from 1.82 to 1.55 was achievable, while still maintaining greater than 90% SO_2 removal, by increasing the sorbent's retention time within the fabric filter (Miller et al., 2000). No significant impact on the filter performance was noted in either test series in which sodium bicarbonate was injected

NO_x Reduction by Sodium Bicarbonate Injection

Some level of NO_x reduction was observed with sodium bicarbonate injection, although the mechanism by which this occurs is not well understood. One possible reaction mechanism is that the combustion products, SO_2 and NO, are catalytically oxidized on the surface to SO_3 and NO_2, respectively. The SO_3 then reacts with available sodium carbonate forming sodium sulfate while the NO_2 reacts to form sodium nitrate. A likely reaction for the capture of NO_2 is the following:

$$Na_2CO_3 + 3NO_2 \rightarrow 2NaNO_3 + NO + CO_2$$

Unlike the SO_3, the NO_2 does not have the ability to diffuse into the particle's interior. Therefore, while the production of SO_3 and NO_2 continues on the surface, the NO_2 is not completely captured, leaving some residual level in the gas stream.

Typical percentages of NO_x removal ranged from 5 – 10% at a NSR of 2.75. These removals, measured with a flue gas temperature of 325°F, indicate some level of NO oxidation and subsequent capture of the NO_2 on the sodium carbonate surface. Additional screening tests performed with a flue gas temperature of 425°F indicated between 10 – 15% of the NO had been oxidized to NO_2, however, no net decrease in NO_x emissions were observed. No explanation is offered for these results since additional studies report that NO_x removals do not decrease until significantly higher temperatures are reached (i.e., 800°F) (Babcock & Wilcox Co., 1999)).

SCR NO_x Conversion

Proposed initial testing included evaluating the low temperature SCR catalyst for NO conversion at several different flue gas temperatures, NH_3/NO molar ratios, and space velocities ranging between 12,000 and 48,000 h^{-1}. However, when a test series performed at a space velocity of 21,000 h^{-1} yielded very low conversions of NO, it was decided that higher space velocity or a shorter residence time would not yield improved levels of NO conversion. Although greater conversions would be expected at lower space velocities, the geometry of the modified baghouse and limited available catalyzed monolith prevented these tests from being conducted.

The inlet and outlet baghouse emissions were recorded during testing and the percent conversion of NO was determined by the following equation:

$$Conversion(\%) = \frac{([NO]_{initial} - [NO]_{final})}{[NO]_{initial}} \cdot 100$$

The results from the initial series of tests evaluating the NO conversion as a function of catalyst temperature at a space velocity of approximately 21,000 h^{-1} and a NH_3/NO molar ratio of 1.0 are given in Figure 3.1.12.

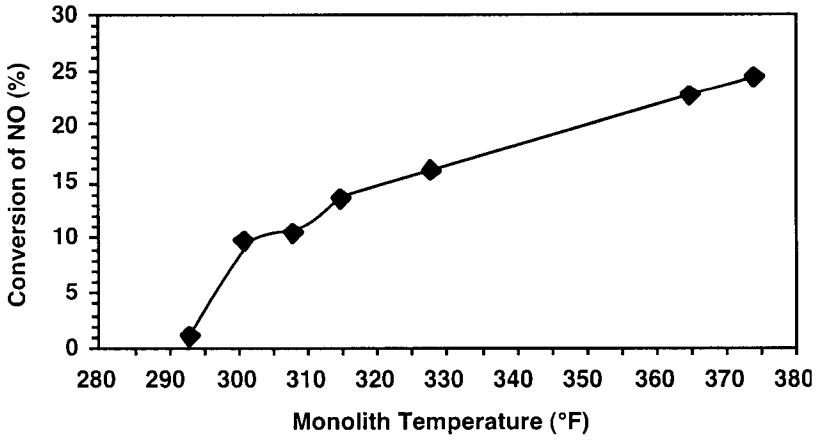

Figure 3.1.12 PERCENT NO_x CONVERSION AS A FUNCTION OF CATALYST TEMPERATURE (space velocity ~21,000 h^{-1}, NH_3/NO molar ratio ~ 1.0)

A maximum NO conversion of 24.3% was achieved at a catalyst temperature of 374°F. Additional test results were measured at temperatures as high as 410°F. However, difficulties in maintaining a steady NO concentration in the flue gas exiting the combustor made these results unreliable. Significant heat loss from the baghouse, combined with the temperature limits of the filter bag fabric, prevented temperatures above 410°F from being achieved. A list of the general operating conditions are provided in Table 3.1.3.

Table 3.1.3 Operating Parameters for SCR Catalyst/Dry Sorbent Injection

Sodium Bicarbonate Injection	
Normalized Stoichiometric Ratio (NSR)	2.75
Air-to-Cloth Ratio	3.0
Time Between Backpulses (sec)	105
Backpulse Pressure (psi)	80
Pressure Drop (inch w.c.)	1.5-2.2
Injection Velocity (ft/sec)	70
Injection Temperature (°F)	300-500
SCR Catalyst	
Cells Per Square Inch (CPSI)	200
Catalyst Volume (ft^3)	0.0478
Catalyst Temperature (°F)	290-410
Pressure Drop (inches water column)	1.2-2.0
NH_3/NO_x Molar Ratio	0.6-1.0

The initial objective of this work was to demonstrate this technology at the industrial scale on Penn State's 15 MM Btu/h watertube boiler. Given that the average temperature inside the baghouse of this facility is 365 °F, while burning the Middle Kittanning seam coal, these results accurately represent the percent NO_x conversion that could be achieved with this technology.

Figure 3.1.13 shows the percent conversion of NO_x versus catalyst temperature measured in the DFC and during the earlier bench scale evaluations. This figure shows that when the space velocities are considered, good agreement exists between the bench scale and the DFC results.

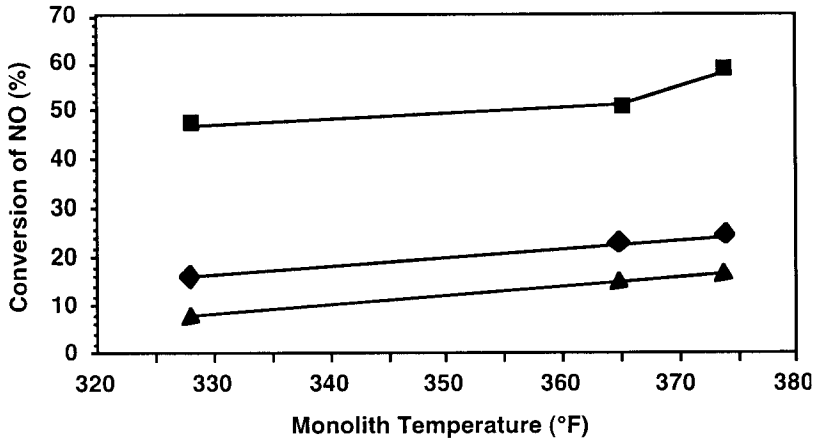

Figure 3.1.13 NO_x CONVERSION VERSUS MONOLITH TEMPERATURE FOR 21,000 H^{-1} (■) IN THE DFC AND 12,000 h^{-1} (◆) AND 24,000 h^{-1} (Δ) IN THE BENCH-SCALE TESTING

Selectivity

The potential exists for the injected ammonia and the nitric oxide (NO) to undergo an additional reaction as follows:

$$4NO + 4NH_3 + 3O_2 \rightarrow 4N_2O + 6H_2O$$

This secondary reaction is not desired, since the product, N_2O, is a greenhouse pollutant. The chemiluminescent NO_x analyzer that was used has the ability to analyze for either NO or NO_2, a further oxidized state of NO. To determine the percent of NO converted by the above reaction, an analyzer was added to measure the N_2O at the baghouse outlet. The selectivity to N_2 was then determined by the following equation:

$$Selectivity(\%) = \frac{([NO]_{initial} - [NO]_{final} - [N_20])}{[NO]_{initial} - [NO]_{final}} \cdot 100$$

Mechanical failures of the analyzer prevented N_2O measurements for several of the tests conducted. However, the selectivity determined for the higher temperatures reported in Figure 1.1.12 was approximately 80%. Earlier work conducted on the bench scale suggests that using lower space velocities would yield higher selectivities (Anand et al., 1997).

Ammonia Slip

The ammonia slip measured at the baghouse outlet was below the detection limits of the ammonia analyzer for all tests performed injecting at a NH_3/NO_x molar ratio of less than or equal to 1.0

Conclusions

Typical combustion control techniques for limiting NO_x emissions from coal-fired utility boilers, such as low NO_x burners, have demonstrated 15-50% reduction in NO_x emissions. However, the application of these techniques in coal-fired industrial boilers is limited due to the small combustion chamber. The short flue gas residence time makes completing combustion when applying staged burners or reburn fuels very difficult. The technology of utilizing a low-temperature SCR catalyst in combination with ammonia injection could provide comparable or additional reductions of NO_x emissions when applied post combustion. Pilot-scale tests have demonstrated that a low temperature SCR catalyst can achieve better than 20% reduction at typical temperatures (365°F) observed inside an industrial or utility-scale baghouse. Although a selectivity of approximately 80% was determined for some of the higher temperatures, earlier work suggests that decreasing the space velocity increases the selectivity. These measurements were made with little or no ammonia slip at space velocities of approximately 21,000 h^{-1}.
The use of dry sorbent injection, such as sodium bicarbonate, can provide not only significant reductions in SO_2 emissions, but provides some added reduction in the NO_x emissions. Greater than 90% reduction in the SO_2 emissions and 5-10% reduction in NO_x emissions was demonstrated at the pilot-scale using a NSR of 2.75. Optimizing the operation of the baghouse backpulsing could lead to further decreases in the NSR. The use of dry sorbent injection further eliminated the possible formation of ammonium bisulfate, a potential source of fouling for the SCR catalyst and down stream equipment.

3.1.2 BioLime™ Injection

The Clean Air Act Amendments (CAAA) of 1990 established the Acid Rain Program under Title IV to achieve significant environmental and public health benefits through reductions in emissions of SO_2 and NO_x from power plants. NO_x emission limits are expected to be

decreased to 0.15 lb/MMBtu from coal-fired units by year 2007 under the Ozone Transport Regulation (OTR). In order to achieve very low emissions, a combination of two or more techniques may have to be used. Therefore, there is a need for an inexpensive and simple method to control NO_x. Reburning is an in-situ combustion modification in which NO_x produced in the main combustion zone is reduced by using a reburning fuel as a reducing agent. The reburning configuration divides the combustion zone into three subzones:

- Main combustion zone, where the main fuel is fired in oxidizing or slightly reducing conditions with approximately 80-85% of the heat released;
- Reburn zone, where a reburn fuel (natural gas, oil, pulverized coal, or biomass) is injected to create a fuel-rich, oxygen deficient zone for NO reduction, and the reburn fuel rate is normally 15-20% of the total heat input; and
- Burnout zone, where additional air is introduced further downstream to oxidize any remaining fuel fragments and complete the combustion.

NO formed in the main combustion zone is partially destroyed by the action of hydrocarbon radicals to form molecular nitrogen and nitrogenous intermediate species such as HCN and NH_3.

Various studies (Chen and Ma, 1996; Spliethoff et al., 1996; Liu et al., 1997; Burch et al., 1991) have documented the role of both homogenous and heterogeneous reactions for NO_x reduction when firing coal. However, Wendt (1995) and Mereb and Wendt (1994) have discounted heterogeneous reactions showing that they have minor contribution towards reburning. The reduction potential of a fuel depends on its ability to produce CH_i radicals to react with NO. Assuming that only homogeneous gas phase reactions participate in the reduction, a higher volatile matter content of the fuel will enhance the NO_x reduction.

The reburning process is reasonably well understood when using coal and natural gas as the reburn fuels (Spliethoff et al., 1996; Liu et al., 1997; Bilbao et al., 1994, 1997; Ashworth et al., 1996; Smart and Morgan, 1994; Kercherer et al., 1994; Adams and Harding, 1998; Burch et al., 1991). However, pyrolysis products of biomass and other biomass-based materials have also been shown to cause NO_x reduction by mechanisms similar to reburning (Rüdiger et al., 1997; Pisupati et al, 1997; Brouwer, 1995). Biomass and biomass-based products offer the advantage of not only reducing SO_2 and NO_x emissions because of low nitrogen and sulfur contents, but also reducing greenhouse gas emissions (N_2O and CO_2).

The composition of the biomass or biomass-based product (lignin, cellulose and hemicellulose content) influences the distribution of pyrolysis products (gas, liquid, char) and hence the reduction of NO_x (Samolada et al., 1990; Zanzi et al., 1996). Hence, a deeper understanding of the composition will help in selection of feedstock to increase the yield of pyrolysis gases that are responsible for reducing NO_x emissions.

From a critical analysis of the literature, the concept emerges that the components of biomass (lignin, cellulose, and hemicellulose) and bio-oils themselves play significant roles in determining the pyrolysis behavior of the feed material (Raveendran et al., 1999; Bhalla and Pisupati, 1999). Also, the basic structure is less significant than the composition. In other words, the way in which these components are bound is not as important as the actual amounts of individual components present in the biomass or bio-oils. Thermo-analytical techniques such as TGA, provide information on chemical composition in a simple and rapid manner. ^{13}C-NMR is also a technique that can be used to study the structure of biomass and biomass based materials. Through a combination of techniques like cross-polarization (CP) and magic angle spinning (MAS), it is possible to obtain high-resolution ^{13}C-NMR spectra of solid samples without the necessity of modifying or degrading the sample.

In this phase of the program, the gas composition from flash pyrolysis of BioLime™, which was produced in an earlier study (Bhalla and Pisupati, 1999) was used to model NO reduction through homogeneous gas phase reactions when BioLime™ was used as a reburn fuel. The numerical predictions were then compared to NO_x emission levels from Penn State's down-fired combustor (DFC) testing to validate the model. A difference in NO_x reduction was observed by using the two different BioLime™ products as reburn fuels under similar operating conditions. This is believed to be due to differences in yields of flash pyrolysis products from the different BioLime™ feedstocks. With this in mind, the model was further used to study the relative contribution of each of the pyrolysis gas species in NO reduction through homogeneous reactions. The predictions were then verified by experimental results from the flow reactor. The composition of two biomass-based materials was studied using TGA and CP/MAS ^{13}C-NMR techniques. Samples were then flash pyrolyzed in a flow reactor to relate the yield of pyrolysis gases and char with the composition.

3.1.2.1 Experimental

Raw Materials

Two biomass-based materials (BioLime™ I and III) were obtained from DynaMotive Technologies Corporation, Vancouver, Canada. BioOil produced from pyrolysis of biomass was simultaneously reacted with air, and lime/water slurry in a stirred reactor to prepare BioLime™. BioLime™ I has approximately 7 wt. % calcium, whereas BioLime™ III has a higher calcium content of approximately 14 wt %. Both samples, as obtained, were highly viscous liquids requiring progressive cavity pumps to induce flow, and had a decomposition temperature of about 60°C (160°F), at which congealing began to occur. The samples were first dried in an oven at 44°C (111°F) overnight. The dried samples were ground to pass though a 60 mesh (US standard) screen and stored in sample bottles. Compositional analysis of the samples is shown in Table 3.1.4.

Table 3.1.4 Compositional Analysis of the Two BioLime™ Samples (wt.%)

	BioLime™ I	BioLime™ III
Carbon (daf[a])s	48.5	38.7
Hydrogen (daf)	7.7	8.4
Nitrogen (daf)	0.23	0.21
Sulfur (daf)	0.01	0.02
Oxygen (daf by diff)	43.5	52.6
Ash (db[b])	20.9	48.5
Moisture (wt. %)	7.97	4.11

[a] dry ash-free basis
[b] dry basis

TGA Study

A Perkin-Elmer 7 series Thermal Analysis System was used for TGA studies on the two BioLime™ samples. Approximately 10 mg of BioLime™ sample was placed in a platinum crucible of the TGA furnace. The quantity of sample was chosen such that the volatile species were removed efficiently from the sample and thereby vapor-phase mass transfer did not control the BioLime™ pyrolysis. The furnace was heated from 30 to 1,000°C at a rate of 50°C min^{-1} and then held isothermally at 1,000°C for 10 minutes. The methodology used was similar to that

reported by Ghetti et al., (1996), Vitolo and Ghetti (1994), and Raveendran et al., (1996). All of the pyrolysis studies were carried out in an inert atmosphere of flowing nitrogen (150 sccm)

Each test yielded a plot of weight loss versus time and temperature. The ash-free weight loss curve for each sample was calculated by subtracting the weight of ash (obtained from the proximate analysis) from the sample weight at each temperature. It was assumed that the weight of ash remains constant during pyrolysis. The percentage weight loss was calculated from the ash-free weight as a function of temperature.

CP/MAS ^{13}C-NMR Study

The solid state ^{13}C NMR spectra, employing the techniques of cross polarization/magic angle spinning (CP/MAS) were collected for BioLime™ samples on a Chemagnetics M100 NMR spectrometer operating at a field strength of 2.3 T. Approximately 250 mg of samples was loaded into a 9 mL ceramic rotor for all the experiments. The rotor was then placed in a spectrometer and accelerated to a spinning rate of 3.5 kHz. All spectra were collected in 0.6 K and zero-filled to 4K over a sweep width of 10 kHz. A contact time of 2 ms and a recycle delay of 1 s were applied with 230,000 transients collected. All shifts were measured relative to tetramethylsilane (TMS). The peaks were then quantified using GRAMS/32 software involving a mixture of Gauss and Lorz integration methods

Flow Reactor Set-up

The experimental setup used for flash pyrolysis is shown in Figure 3.1.14. Flash pyrolysis was performed in a flow reactor of length 137 cm (54 inches) and 3.8 cm (1.5 inches) ID Schedule 40 stainless steel 316 pipe. The reactor was heated using a Lindberg® model 55342 single-zone furnace. The furnace was interfaced to a Lindberg® controller capable of achieving and maintaining any temperature between 200 and 1,200°C. Samples were pyrolyzed at peak temperatures of 1,100 and 1,200°C. The peak temperatures were selected to be consistent with the temperatures found in the reburn zone of the pulverized coal-fired combustor. In each run, approximately 2 grams of sample were pyrolyzed using helium as carrier gas at a flow rate of 0.707 m^3(std.)/h (25 scfh) to achieve a heating rate of 600°C/second when passed through the hot zone of the reactor. The pyrolysis products leaving the reactor were passed through a 2μm filter paper to collect the char. The char was collected from the filter paper and weighed. The gases

were collected in a 10-liter TEDLAR® bag and were later analyzed using an Arnel 0158 Series S GC. The peaks were integrated and quantified (based on 1 ml sample injected) using Chrom Perfect, version 3.5 software. The gas composition was then calculated as milligrams/gram of BioLime™ sample using gas densities at 25°C.

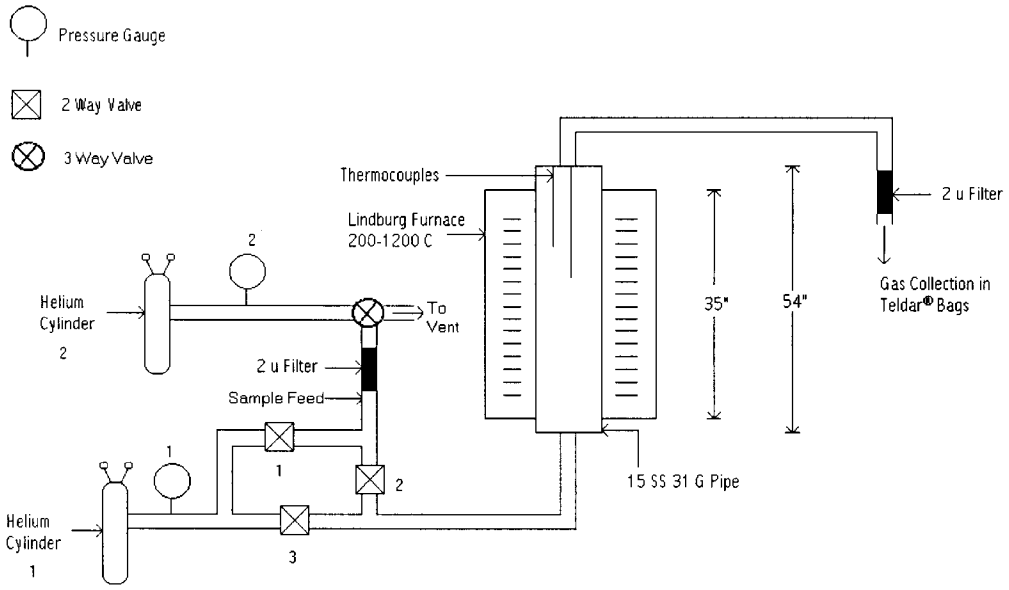

Figure 3.1.14 SCHEMATIC DIAGRAM OF THE FLOW REACTOR USED FOR FLASH PYROLYSIS

3.1.2.2 Down-Fired Combustor (DFC)

The DFC, shown in Figure 3.1.1 and discussed in Section 3.1.1.1, was used to evaluate SO_2 and NO_x emissions when using BioLime™ in a pilot-scale combustor. BioLime™ was introduced through port 5 into the reburn zone. Wall temperatures were monitored with type-S thermocouples at six locations along the combustor. Table 3.1.5 provides the ultimate analysis of the Middle Kittanning seam coal used in the study. The reburn zone parameters are shown in

Table 3.1.6. The BioLime™ was prepared, stored in a day tank, and pumped to the burner by a Moyno™ progressive cavity pump. The flue gas composition (O_2, CO_2, CO, SO_2, and NO_x) was recorded using a Texas Micro Systems™ Data Acquisition System with ViewDac™ software. The data collected during steady-state operation was then averaged.

Table 3.1.5 Analysis of the Middle Kittanning Seam Coal used in the Testing

Constituent	Weight % (Dry basis)
Carbon	77.32
Hydrogen	4.89
Nitrogen	1.22
Sulfur	2.13
Oxygen	1.53

Table 3.1.6 DFC Reburn Zone Parameters

DFC Reburn zone parameters	
Diameter	50.8 cm
Total length	96.52 cm
Volume	195,600 cm^3
Pressure	1 atm
Residence time	1.127 seconds
Inlet temperature at the center	1415 K
Inlet temperature at the wall	1426 K

3.1.2.3 Results and Discussion

TGA Results

Proximate analysis showed that both BioLime™ samples have different ash contents and hence, the unsubtracted weight loss curves obtained directly from the TGA are not directly comparable for determining volatiles yield. The weight loss curves on an ash-free basis shown in Figures 3.1.15 and 3.1.16 for BioLime™samples I and III, respectively. The curves can be divided into four zones (Ghetti et al., 1996; Raveendran et al., 1996). These four zones can thus be related to the decomposition of individual components of BioLime™ as shown in Table 3.1.7. Various zones arise from the fact that lignin, having an aromatic structure, is expected to undergo pyrolysis at a higher temperature than that for cellulose and hemicellulose, which are saturated compounds.

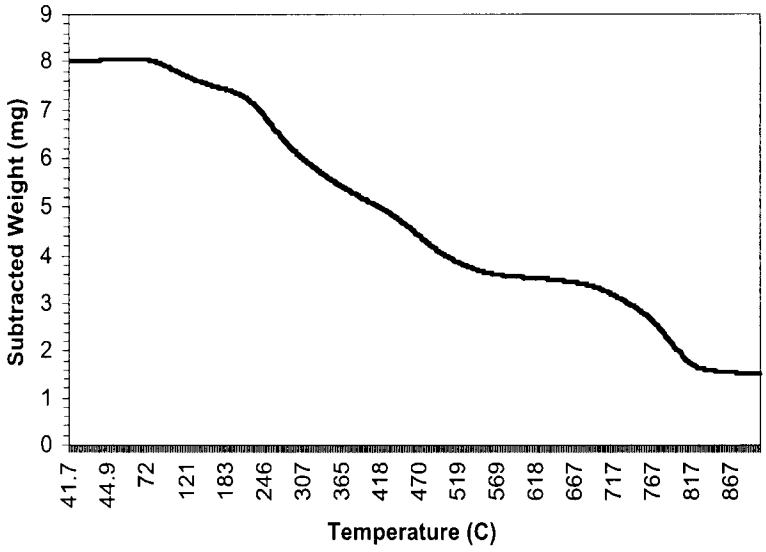

Figure 3.1.15 ASH-FREE WEIGHT AS A FUNCTION OF TEMPERATURE FOR BioLime™ I

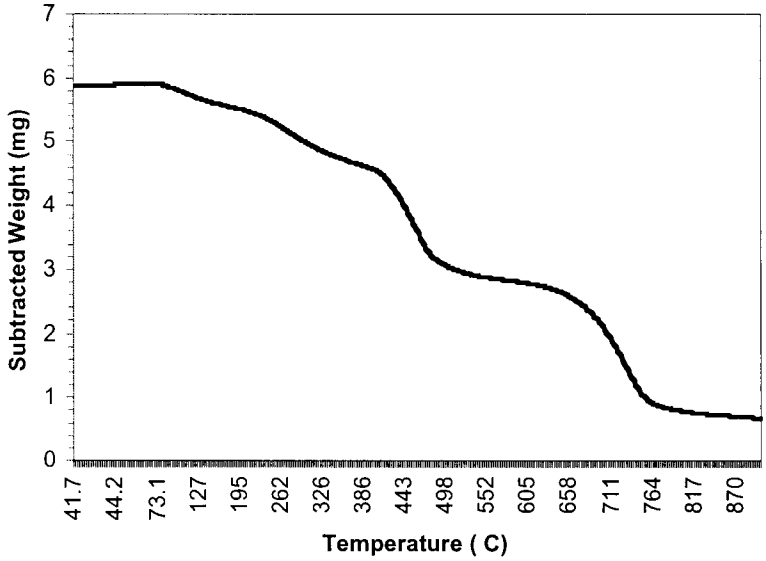

Figure 3.1.16 ASH-FREE WEIGHT AS A FUNCTION OF TEMPERATURE FOR BioLime™ III

Table 3.1.7 Various Zones of Weight Loss during the Pyrolysis of BioLime™ Samples

Zones	Corresponding Component
Zone I: ~100°C	Mainly moisture evaporation
Zone II: 166-400°C	Predominately hemicellulose and cellulose decomposition
Zone III: 400-600°C	Mainly lignin decomposition
Zone IV: 600-900 C	Thermal cracking of char

The distribution of moisture and volatile matter as a percent of total ash-free weight during pyrolysis is shown in Table 3.1.8. Table 3.1.9 shows the weight loss for both samples in Zones II and III as a fraction of initial weight.

Table 3.1.8 Cumulative Volatile Matter Yield (wt.%) during Pyrolysis of BioLime™ I and III

Zones	BioLime™ I	BioLime™ III
Zone I (~100°C) Moisture	8.36	5.77
Zone II (166-400°C) Hemicellulose and Cellulose	35.95	19.09
Zone III (400 –600°C) Lignin	24.26	34.30
Zone IV (600-900°C) Secondary thermal decomposition of char	31.40	40.83
Total volatiles released in (Zone II + Zone III)	60.21	53.40
Total volatiles released (Zone II +Zone III + Zone IV)	91.61	94.23

Evaluation of the weight loss of the samples between 166 and 900°C indicated that approximately 83% of the volatile matter, as determined from the proximate analysis, was released in the interval. Knowing that the individual components (hemicellulose, celluolose, lignin) play a more significant role in determing the pyrolysis characteristics of BioLime™ than the basic structure or degree of polymerization, the zonal distribution of volatiles released can be used to compare the amounts of individual components present in the BioLime™. Data

Table 3.1.9 Percent Volatile Matter Released in Zones II and III for the BioLime™ Samples

	BioLime™ I (weight loss/Initial Weight x 100)	BioLime™ III (weight loss/Initial Weight x 100)
Zone II	22.46	8.35
Zone III	15.15	15.0
Total	37.61	23.35

presented in Table 3.1.8 indicate that BioLime™ I has higher cellulose and hemicellulose contents, whereas BioLime™ III has higher lignin content. A higher amount of weight loss in Zone IV for BioLime™ III indicates that the higher lignin content forms more char during pyrolysis. More volatiles are released by primary pyrolysis for BioLime™ with a lower lignin content. A higher sum of percent distribution for zones II and III for BioLime™ I corroborates this point.

CP/MAS ^{13}C-NMR Results

The NMR spectra for BioLime™ I and III are shown in Figures 3.1.17 and 3.1.18, respectively. The signal assignments for the chemical shifts in the spectra are summarized in Table 3.1.10, based upon values reported by others (Pfeffer and Gerasimonwicz, 1989; Macial et al., 1984; Haw et al., 1984; Sterk, 1987; Cyr et al., 1988; Almendros et al., 1992; Landuci et al., 1992, Love et al., 1992; Pan and Lachenal, 1995; Haw and Schultz, 1985). The relative intensities of the peaks as obtained from GRAMS/32 software are also shown in Table 3.1.10.

The following observations can be made from the data in Table 3.1.10:

- The peak at 148-149 ppm in the spectra is due to C_3 and C_5 of syringyl units, but only those with a free phenolic group at C_4. The peak at 153 ppm, which is also due to C_3 and C_5 of syringyl units but with ether linkages at C_4 (principally C_β-O-C_4 bond), is completely absent from the spectra. This indicates that aryl-alkyl ether linkages of the lignin are almost completely cleaved during the pyrolysis;
- The peaks at 181 (ester and carboxylic acids) and 148-149 (phenolic carbon) ppm show that both the BioLime™ samples have significant concentrations of oxygenated compounds;
- No cleavage of lignin methoxy groups and major reorganization of the aromatic rings takes place during the pyrolysis of biomass to form BioLime™; and

- The signals due to the aromatic carbon of lignin are well separated from the signals due to carbohydrates (although minor overlap with the signal due to C-1 of cellulose is present). A relative measure of lignin aromatic carbon content can be obtained by integrating from approximately 160-ppm to the low shielding side of the C-1 peak (approximately 109-ppm) (Haw et al., 1984).

The intensity of the region from 160-109 ppm can be calculated (Haw et al., 1984) for both BioLime™ I and III and is referred to as I_{low}. A formula of $C_9H_{8.35}O_{2.83}(OCH_3)_{1.43}$ with a formula weight of 206 g/mol is assumed to be representative of the lignin (Rydholm, 1965). Carbohydrates repeat units have an average empirical formula of $C_6H_{10}O_5$ (formula weight 162 g/mol). This assumption is completely valid for cellulose and approximately valid for hemicellulose. With this assumption, total integrated ^{13}C intensities due to all lignin and all carbohydrate carbons, I_{lig} and I_{carb} were calculated as:

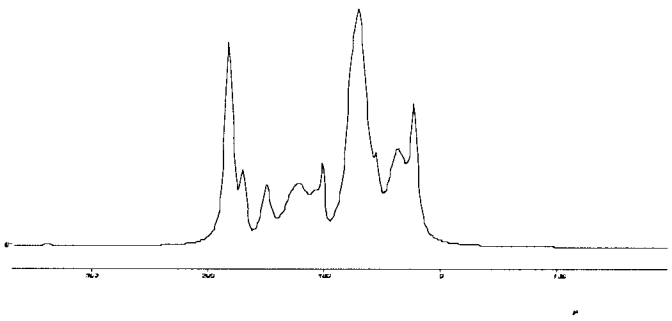

Figure 3.1.17 ^{13}C-NMR SPECTRA FOR BioLime™ I

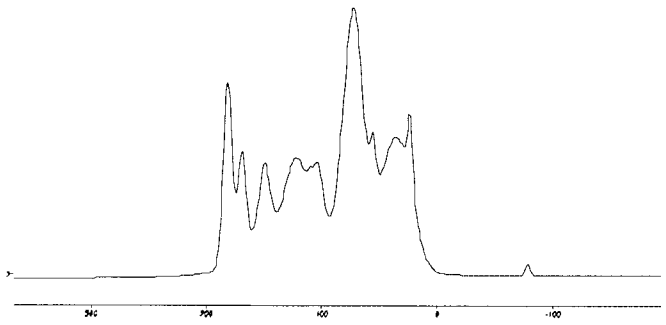

Figure 3.1.18 ^{13}C-NMR SPECTRA FOR BioLime™ III

Table 3.1.10 Signal Assignment and Percent Intensity of Chemical Shifts in ^{13}C-CP/MAS NMR Spectra of BioLime ™ Samples

Peak Shift (ppm)	Assignment	BioLime™ I (Intensity %)	BioLime™ III (Intensity %)
181	Esters & carboxylic acids	17.0	8.55
168-169	carbonyl atoms of hemicellulose	2.3	5.64
148-149	Aromatic lignin C bonded to O	5.6	10.6
120-109	Aromatic lignin bonded to C or H	11.7	18.1
69-103	Cellulose carbon	42.4	38.1
54-58	OCH_3 group of lignin	1.8	2.6
30-40	alkyl C of lignin not attached to O	10.1	18.9
22-23	CH_3 of acetyl group of hemicellulose	9.3	3.0

$$I_{lig} = (10.43/6) \times I_{low} \qquad 3.1.1$$

Equation 3.1.1 follows directly from the assumption that the average lignin repeat units has 10.43 carbons, 6 of which account for the total intensity measured by I_{low}.

$$I_{carb} = (100 - I_{lig}) \qquad 3.1.2$$

The wt.% of lignin can then be calculated as follows:

$$\text{Wt \% lignin } 100\times[(206/10.43) \times I_{lig}/\{(206/10.43) \times I_{lig}+(162/6) \times I_{carb}\}] \qquad 3.1.3$$

The I_{lig} and weight % of lignin calculated from equation 3.1.3 is shown in Table 3.1.11.

Table 3.1.11 I_{lig} and Weight Percent of Lignin Calculated for BioLime™ I and III

	I_{lig}	Weight % Lignin
BioLime™ I	30.07	23.9
BioLime™ III	50.1	42.0

Both ^{13}C-NMR and TGA analyses show that BioLime™ I has a lower lignin content (higher cellulose and hemicellulose content) than BioLime™ III. As seen from the TGA analyses, lower lignin content releases more volatiles by primary pyrolysis. Since BioLime™ is flash pyrolysed upon injection into the combustor, primary pyrolysis is thus predominately responsible for release of volatiles, which then react with NO reducing it to N_2.

Flow Reactor Results

The composition of pyrolysis products from the flow reactor, calculated in milligrams/gram of BioLime™ is shown in Table 3.1.12. The total yield as well as the yield of the individual gases is higher for BioLime™ I. BioLime™ III is observed to produce more char. This pyrolysis behavior of both BioLime™ I and III is consistent with the lignin, cellulose, and hemicellulose contents calculated from the TGA and ^{13}C-NMR analyses. In other words, BioLime™ I, which has higher cellulose and hemicellulose content, produced more volatiles by primary pyrolysis. A higher lignin content in BioLime™ III forms more char during pyrolysis. Also, the weight percent of the total gas yield from flash pyrolysis closely matches the weight loss of BioLime™ in Zone II and Zone III in Table 3.1.9. This proves that primary pyrolysis is mainly responsible for the volatiles evolved during the flash pyrolysis. The weight percent of total gas yield for BioLime™ I is 1.7 times that for BioLime™ III, which also closely matches the lower lignin content (1.75 times) calculated from ^{13}C-NMR (Table 3.1.11)

Table 3.1.12 Composition of Pyrolysis Products at 1,100°C

Product	BioLime™ I (mg/g of BioLime™)	BioLime™ III (mg/g of BioLime™)
Hydrogen (H_2)	3.37	2.95
Carbon dioxide (CO_2)	278.21	158.77
Carbon monoxide (CO)	41.22	25.29
Methane (CH_4)	8.79	6.34
Ethane (C_2H_6)	1.46	0.86
Ethylene (C_2H_4)	8.19	5.53
Acetylene (C_2H_2)	0.77	0.51
Total	342.0	200.3
Total wt. % gas yield	34.20	20.02
Char	409	572
Total wt. % char yield	40.9	57.2

The composition of gases and char in milligrams/gram of BioLime™ III at 1,100 and 1,200°C is shown in Table 3.1.13. The decrease in char yield with increasing temperature is due to secondary decomposition of the char residue. The gaseous product yield increased with peak pyrolysis temperature. The increase in gaseous products can be attributed predominately to secondary decomposition of the char at higher temperatures. However, secondary decomposition of the char at higher temperatures may also give non-condensable gaseous products. The yields of CO, CO_2, and H_2 increased in general with increasing temperature. However, the increase in yield of CO_2 is more pronounced than that of CO or H_2. A slight decrease in yield of hydrocarbon gases is observed with increased temperature. The results are consistent with work reported in the literature by Rüdiger et al., (1997) Horne and Williams (1996).

Modeling NO_x Reduction

All numerical calculations were performed using a PSR computer code (Glarborg et al., 1989), which runs in conjunction with the Chemkin library (Kee et al., 1989). The reverse rate constants were obtained from the forward rate constants and the thermodynamic data was mainly taken from the Sandia Thermodynamic Database (1987). The code computes species concentrations from the balance between the net rate of production of each species by chemical reaction and the difference between the input and output flow rates of species. The model used to predict NO emissions is taken from the studies of Kilpinen et al., (1992) and Glarborg et al.,

Table 3.1.13 Composition of Pyrolysis Products for BioLime™ III at 1,100 and 1,200°C

Product	1,100°C (mg/g of BioLime™)	1,200°C (mg/g of BioLime™)
Hydrogen (H_2)	2.95	3.76
Carbon dioxide (CO_2)	158.77	191.27
Carbon monoxide (CO)	25.29	44.61
Methane (CH_4)	6.34	6.08
Ethane (C_2H_6)	0.86	0.86
Ethylene (C_2H_4)	5.53	5.39
Acetylene (C_2H_2)	0.51	0.799
Total	200.2	252.7
Total wt. % gas yield	20.02	25.27
Char	57.2	517
Total wt. % char yield	57.2	51.7

(1989). In general, the mechanism includes generation of hydrocarbon radicals from C_1 and C_2 parent hydrocarbons, oxidation mechanisms for HCN, and NH_3, together with a subset of the interactions between the hydrocarbon radicals and the nitrogenous species. The nitrogen-hydrocarbon chemistry is essentially an extension of the Miller and Bowman mechanism (1989). The procedure and assumptions in the BioLime™ study are:

- Only homogeneous gas phase reactions are responsible for NO reduction. The effect of heterogeneous reactions is neglected. Gases from the pyrolysis of BioLime™ react with NO_x in the reburn zone to form N_2 and nitrogenous intermediate species such as HCN and NH_3;
- Gas concentrations are calculated from the yields reported in an earlier study (Bhalla and Pisupati, 1999) and are shown in Table 3.1.12 from flash pyrolysis for BioLime™ I and III;
- Reburn fuel is mixed rapidly and perfectly with the products of combustion from the primary zone. This is achieved by use of a high-pressure injection nozzle for feeding the reburn fuel;
- Reburn fuel is pyrolyzed instantly on entering the combustor and therefore pyrolysis kinetics do not control the NO_x reduction kinetics;
- The kinetics of reburning are controlled by the rate constants for the hydrocarbon-NO reaction system. The effect of mass transfer is neglected. This follows from the previous two assumptions;
- An average of the wall and bulk temperatures at the point of reburn fuel injection is used as the inlet temperature for the calculations;
- Gas densities are calculated at the reburn zone inlet temperatures;
- The flue gas in the reburn zone consists of 14% CO_2, 2.0% O_2, and 497 ppm of CO in nitrogen. These concentrations of CO_2, O_2, and CO are chosen to be consistent with those of a coal primary flame operated at a stoichiometric ratio of 1.0-1.1; and

- A residence time of 1.127 seconds is used for the calculations, which is consistent with the residence time in the reburn zone of the DFC.

Discussion of Results

Predictions of NO_x emissions from the model along with the DFC data are shown in Table 3.1.14. The reburn zone stoichiometry is based on the total amount of fuel and oxidizer that enters the DFC in the first two zones of the combustor divided by the stoichiometry requirement for the primary and reburn fuel. The stoichiometry requirements for coal and BioLime™ were calculated by subtracting the amount of air equivalent to oxygen in the fuel from the amount of air required for complete oxidation of carbon and hydrogen (determined by the ultimate analysis) content of the fuel. The predictions from the model match closely with the DFC data. The results show a higher NO_x reduction for BioLime™ I than for BioLime™ III. However, the stoichiometry was different for different runs when BioLime™ I and III were used as reburn fuels. Therefore, to further compare the performance of BioLime™ I and III, NO_x reduction was estimated for both BioLimes™ for each run. The results are shown in Figure 3.1.19. It can be seen that BioLime™ I, shows a higher NO_x reduction than BioLime™ III, which is attributed to the higher yield of total pyrolysis gases for BioLime™ I, which is in agreement with the studies of Kicherer et al., (1994). Kircherer et al. showed that the main reduction effect is due to the volatiles of the reburning fuel. Therefore, a higher yield of pyrolysis gases will result in higher NO_x reduction.

Table 3.1.14 Model Predictions for Percentage NO_x Reduction with NO_x Reduction Observed in the DFC

Run (BioLime™)	Stoich-iometry	% of Hydro-carbon added	% CO_2 added	% CO added	% H_2 added	% NO_x Reduction (DFC)	% NO_x Reduction (Model)
Run 1(I)	0.501	0.13	14.88	0.25	0.23	17.0	16.0
Run 2(I)	0.517	0.14	14.92	0.26	0.24	16.2	16.8
Run 3(III)	0.549	0.09	14.50	0.18	0.20	13.6	11.2
Run 4(III)	0.652	0.04	14.20	0.10	0.08	11.6	4.4
Run 5(III)	0.656	0.05	14.27	0.12	0.11	12.5	7.2
Run 6(III)	0.717	0.05	14.27	0.12	0.11	12.6	6.3

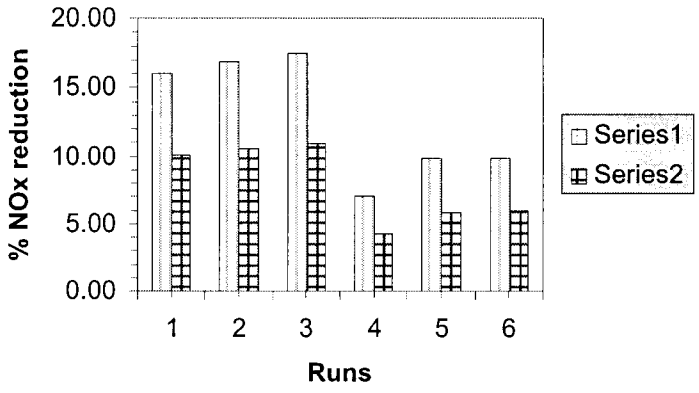

Figure 3.1.19 INFLUENCE OF BioLime™ USED ON NO_x REDUCTION. THE PERCENT NO_x REDUCTION IS PREDICTED FROM THE MODEL FOR BOTH BioLime™ FOR EACH RUN CONDITION. (Series 1 – BioLime™ I, Series 2 - BioLime™ III)

Different pyrolysis gases have different NO_x reduction potential. However, as seen from Table 3.1.14, the relative percentage of pyrolysis gases added is different for different runs. Knowledge of the relative contribution of pyrolysis gases in NO_x reduction will help in the selection of a biomass feedstock to increase the yield of desired species. With this in mind, a parametric analysis was performed using the model to study the effect of varying concentration of hydrocarbons, CO_2, CO, and H_2. The results were then verified using the flow reactor. The setup of the flow reactor is discussed in an earlier study (Bhalla and Pisupati, 1999). The results are shown in Figures 3.1.20 to 3.1.23. The results show that CO_2, CO, and H_2 have very little effect on NO_x reduction. Hydrocarbons are seen to be mainly responsible for causing reductions in emissions of NO_x. Kilpinen et al., (1992), Chen et al., (1986), and Mereb and Wendt (1990) have also shown that for natural gas reburning CO, and H_2 are useable as reburn fuels, even though the rates of reaction for NO reduction by CO and H_2 are significantly slower compared to NO-hydrocarbon reactions. Two main stages are considered to be mainly responsible for nitric oxide reduction. First is the destruction of NO to HCN, through the reaction with CH_i and HCCO.

$$NO + HCCO \rightarrow CNO + H \rightarrow HCN$$

$$NO + {}^1CH_2 \rightarrow HCN + OH$$

$NO + CH_3 \rightarrow H_2CN + M \rightarrow HCN$

$NO + CH_3 \rightarrow HCN + H_2O$

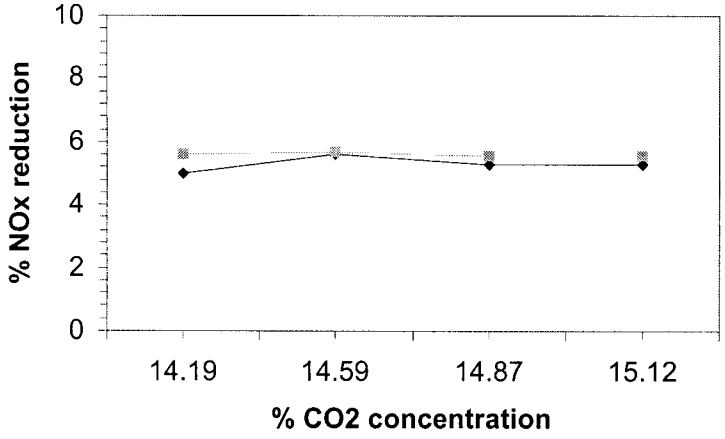

Figure 3.1.20 EFFECT OF CO_2 CONCENTRATION ON NO_x REDUCTION (■ Experimental, ◆Model A)

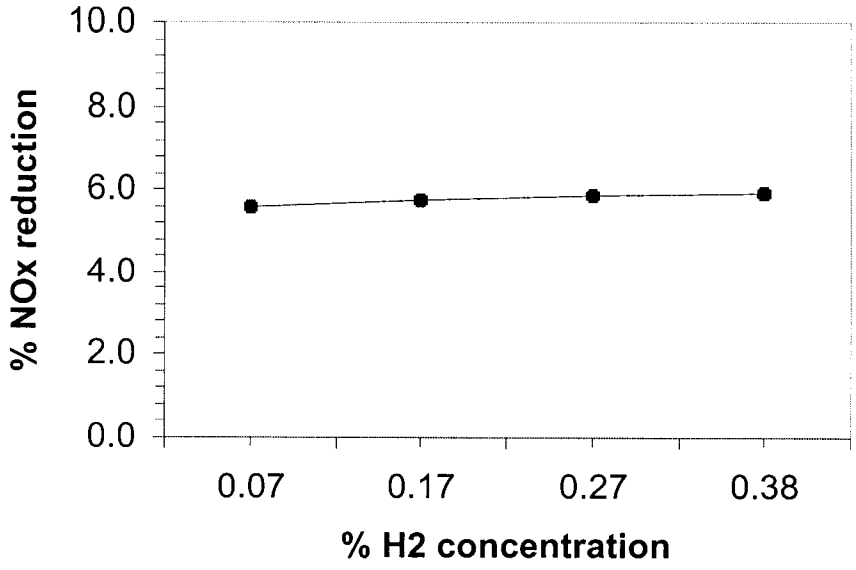

Figure 3.1.21 EFFECT OF H_2 CONCENTRATION ON NO_x REDUCTION (using Model A)

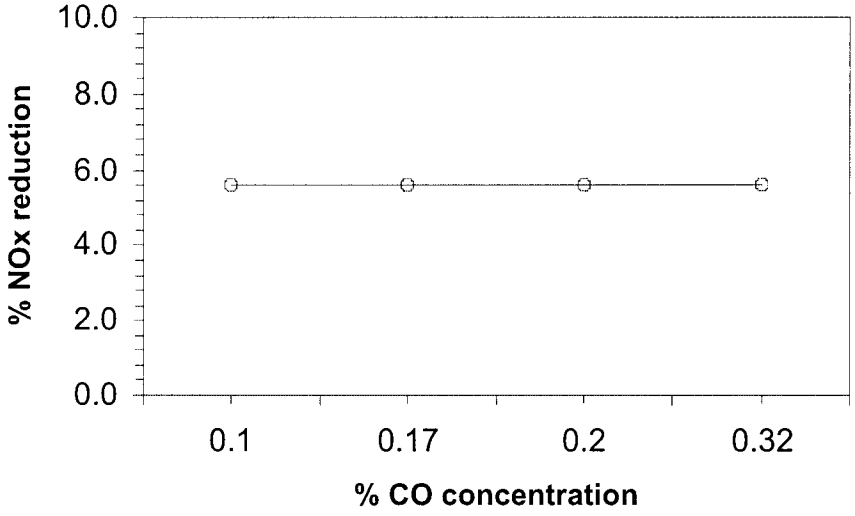

Figure 3.1.22 EFFECT OF CO CONCENTRATION ON NO_x REDUCTION (using Model A)

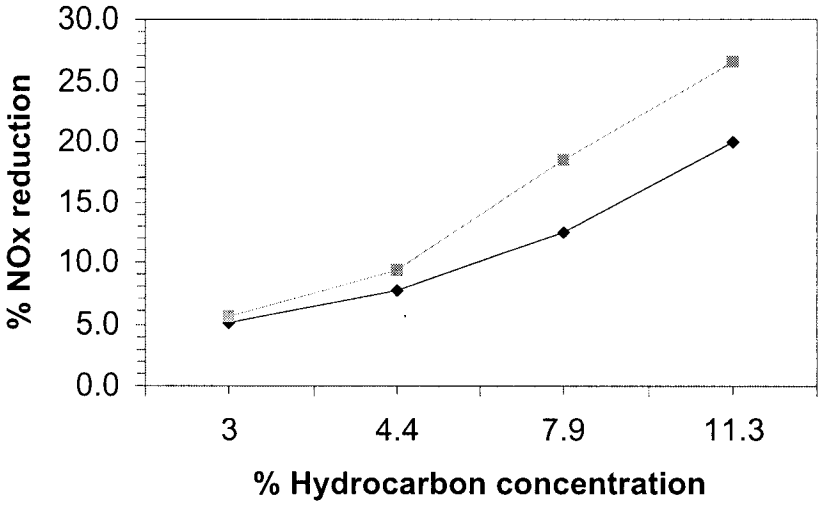

Figure 3.1.23 INFLUENCE OF HYDROCARBON CONCENTRATION ON PERCENT NO_x REDUCTION (■ Experimental, ◆ Model A)

The second stage is the reaction of HCN with the oxidizing species (O, OH) to form NH_i, N_2, and NO. HCN is first converted to isocyanic acid, HNCO primarily by

$$HCN + OH \rightarrow HOCN + H \rightarrow HNCO$$

and to a lesser extent also through the direct reaction

$$HCN + OH \rightarrow HNCO + H$$

The HNCO reacts further to NH_2. This occurs primarily by the reaction with a H radical

$$HNCO + H \rightarrow NH_2 + CO$$

The NH_2 radical, depending on the conditions, can be converted to N_2, NH_3, or NO.

Burch et al., (1991) from their study of different fuels (methane, hexane, benzene, and coal) have also shown that NO_x reduction efficiency can be related to C/H ratio for the fuel. Carbon rich fuels produce more CH_i fragments, leading to a lower NO_x concentration. BioLime™ I has a C/H ratio of 6.3 as compared to BioLime™ III which has a C/H ratio of 4.6. Therefore, a BioLime™ with a higher C/H ratio will help to increase the NO_x reduction.

3.1.2.4 Conclusions

The following conclusions were made from the BioLime™ study:

- ^{13}C-NMR and TGA analytical techniques can be effectively used to estimate various components (lignin, cellulose, and hemicellulose content) of biomass-based materials;
- The NMR spectra of the oils indicated that aryl-alkyl ether linkages of the lignin structure are extensively cleaved and carbonyl functional groups were dominating in the BioLime™;
- The TGA weight loss curves of BioLime™ samples in an inert atmosphere showed two distinct peaks between 160-400°C and 400-600°C, corresponding to the decomposition of cellulose, hemicellulose and lignin structures, respectively. The third distinct peak between 600-900°C corresponds to secondary thermal decomposition of the char;
- The total gas yield from flash pyrolysis for both BioLime™ I and III closely matched with the primary pyrolysis weight loss in TGA showing that primary pyrolysis reactions were mainly responsible for the volatiles being evolved in flash pyrolysis;
- Lower lignin and higher cellulose and hemicellulose contents are desirable in choosing a feedstock for NO reduction. Lower amounts of lignin evolved more volatiles and produced less char during flash pyrolysis of bio-oils in the combustor. Higher yields of pyrolysis gases increased the NO reduction potential of the BioLime™ through homogeneous gas phase reactions;

- An increase in pyrolysis temperature increased the gas yield and decreased the yield of char. This is mostly attributed to the increased primary decomposition of the char residue;
- Percentage of NO_x reduction using BioLime™ as a reburn fuel can be accurately predicted using the homogeneous gas phase reaction model. For most of the conditions, the percentage NO_x reduction predicted from the model is well within the allowable variation from the experimental results from the DFC and flow reactor;
- The higher NO_x reduction potential of BioLime™ I over BioLime™ III can be attributed to the higher yield of total pyrolysis gases; and
- The parametric study from the flow reactor shows that the CO, CO_2, and H_2 have very little effect on NO_x reduction and hydrocarbon reactions are mainly responsible for NO_x reduction. Hence a fuel with higher C/H ratio will produce more CH_i fragments, and result in a better NO_x reduction potential.

3.1.3 Reburning

3.1.3.1 Objectives

The main objective of this study was to understand the mechanism by which NO_x emissions are lowered when cofiring coal and coal-water slurry fuel (CWSF) as compared to firing coal only. This was accomplished by obtaining quantitative data to:

- Examine the extent of reburing in the gas phase, and
- Understand the heterogeneous char NO contribution to the reduction of NO.

3.1.3.2 Background

NO_x Fundamentals

Nitrogen oxides emissions from coal combustion can occur from three sources – thermal NO_x, fuel NO_x, and prompt NO_x. Thermal NO_x primarily forms from the reaction of nitrogen and oxygen in the combustion air. Fuel NO_x is a component that forms mainly from the conversion of nitrogen in the fuel to nitrogen oxides. Prompt NO_x is formed when hydrocarbon radical fragments in the flame zone react with nitrogen to form nitrogen atoms, which then form NO.

No definite rules exist to determine which nitrogen oxide formation mechanism dominates for a given stationary combustor configuration because of the complex interactions between burner aerodynamics, and both fuel oxidation and nitrogen species chemistry. But in general, fuel nitrogen has been shown to dominate pulverized coal fired boilers, although thermal

NO is also important in the post-flame regions where over-fire air is used. Thermal NO contributions only become significant at temperatures above 2,500°F in coal flames. Prompt NO formation is not typically an important mechanism during coal combustion. In the absence of fuel nitrogen, fuel NO is not a problem for natural gas flames. Prompt NO, however, is important in the vicinity of the inlet burners where reacting fuel fragments mix with the oxidizing air. Thus, in natural gas burners, both prompt and thermal NO contribute to the formation of nitrogen oxides.

Thermal NO

The principal reactions governing the formation of thermal NO are:

$$N_2 + O \leftrightarrow NO + N \qquad (3.1.4)$$

$$N + O_2 \leftrightarrow NO + O \qquad (3.1.5)$$

These two reactions are usually referred to as the thermal-NO formation mechanism or the Zeldovich mechanism. In fuel-rich environments, it has been suggested that at least one additional step should be included in this mechanism:

$$N + OH \leftrightarrow NO + H \qquad (3.1.6)$$

The reactions (3.1.4), (3.1.5) and (3.1.6) are usually referred to as the extended Zeldovich mechanism. Experiments have shown that as the complexity of the reactors and fuels increase, it is difficult to evaluate the rate forms (Bonvini et al., 1991). The general conclusion is that although the non-quilibrium effects are important in describing the initial rate of thermal-NO formation, the accelerated rates are still sufficiently low that very little thermal NO is formed in the combustion zone and that the majority is formed in the post flame region where the residence time is longer.

Prompt NO_x

Prompt NO_x occurs by the fast reaction of hydrocarbons with molecular nitrogen in fuel-rich flames. This mechanism accounts for rates of NO formation in the primary zone of the reactor, which are much greater than the expected rates of formation predicted by the thermal NO mechanism alone. NO measurements in both hydrocarbon and non-hydrocarbon flames have been interpreted to show that prompt NO is formed only when hydrocarbon radicals are available. The amount of NO formed in the fuel-rich systems is proportional to the concentration of N_2 and also to the number of carbons present in the gas phase. Hence, this mechanism is much more significant in fuel-rich hydrocarbon flames or in the reburning flames. Two reactions are believed to be the most significant to this mechanism (Miller and Bowman, 1989):

$$CH + N_2 \leftrightarrow HCN + N \qquad (3.1.7)$$

$$C + N_2 \leftrightarrow CN + N \qquad (3.1.8)$$

Reaction (3.1.7) was originally suggested and reaction (3.1.8) is considered to be only a minor, but non-negligible, contributor to prompt NO with its importance increasing with increasing temperature (Miller and Bowman, 1989).

Fuel NO

Fuel NO is by far the most significant source of nitric oxide formed during the combustion of nitrogen-containing fossil fuels. Fuel NO accounts for 75 to 95% of the total NO_x accumulation in coal flames and greater than 50% in fuel oil combustors. The reason for fuel NO dominance in coal systems is because of the moderate temperatures (1,500-2,000 K) and the locally fuel-rich nature of most coal flames. Fuel NO is formed more readily than thermal NO because the N-H and N-C bonds common in fuel-bound nitrogen are weaker than the triple bond in molecular nitrogen which must be dissociated to produce thermal NO.

The main step, at typical combustion temperatures, consists of conversion of fuel nitrogen into HCN, a step which according to some investigators (Fenimore, 1976; Rees et al.,

1981) is independent of the chemical nature of the initial fuel nitrogen. Once the fuel nitrogen has been converted to HCN, it rapidly decays to NH_i (i = 1, 2, 3) which reacts to form NO and N_2.

3.1.3.3 NO_x Control Technologies

In order to comply with the regulations for nitrogen oxides emissions, various abatement strategies have been developed. These strategies can be divided into the following categories: 1) modification of the combustion configuration, 2) injection of reduction agents into the flue gases, and 3) treatment of the flue gas by post-combustion de-nitrification processes. A determination of the most effective and least expensive abatement technique depends on specific boiler firing conditions and the emission standards. A combination of techniques may be necessary to achieve certain mandated limits. Hence, the best NO_x control strategy for a certain unit is highly site dependent. Also, the selection of a pollution control system must also include the impact on boiler efficiency since many of the possible changes affect the fuel oxidation process. The large variety of combustion configurations and different fuel types requires that the abatement strategy be applied on a case-by-case basis. Due to complex interactions among fluid dynamics, chemistry, and energy transport processes, there is no guarantee that a particular alternative will achieve the desired control level. For this reason, a combination of theoretical, practical, and computational techniques is highly desirable in the development of a NO_x abatement strategy.

Modifications recognized as being technically viable and effective in reducing nitrogen oxide emissions from 50-80 % include: low excess air, flue gas recirculation, staged air combustion and staged fuel combustion. Also, advanced techniques like AGR-advanced gas reburning (Folsom et al., 1994), advanced low-NO_x burners (De Jong, 1993; Penterson and Ake, 1998) and COMBINOX (Gallo, 1994) have been developed. They usually involve a combination of techniques to reduce NO_x emissions.

Reburning Concept Development and Evolution

Reburning is a combustion modification technology, which removes NO_x from combustion products by using reburn fuel as the reducing agent. This technology is alternately referred to as "in-furnace NO_x reduction" or "staged fuel injection".

The concept was originally developed by the John Zinc Company, and Wendt et al. (1973) and was based on the principle of Myerson et al. (1957) that CH fragments can react with NO. More recently, detailed studies have been conducted on the reburning process, and its potential for large-scale applications has been demonstrated (Chen et al., 1986; Lanier et al., 1986; Mereb and Wendt, 1990; Folsom et al., 1996; Maly et al., 1997; Falcone Miller, et al., 1996; Farzan et al., 1997). Despite these successful demonstrations, implementation of the technology has not been extensive on full scale in power plants, particularly in coal-fired units due to inherent difficulties in optimization of the reburning process. Concerted efforts to develop reburning for application to large boilers started in Japan during the late 1970's and early 1980's. An extensive development effort concerned the Mitsubishi Advanced Combustion Technology, which was applied to full scale boilers and resulted in 50% NO reduction, independent of fuel type and initial NO level. A review of the most representative reburning studies is presented in Table 3.1.15.

Table 3.1.15 Parameters and Characteristics of Reported Reburning Experiments

Recent Citation	**Reburn fuels[a]**	**Combustor Type / No.of exp.**	**NO meas. and reduction**	**Numerical modeling - NO prediction**	**RZ[b] residence time (sec)**	**RZ reburn temp. (°F)**
Chen et al. (1986)	NG	3 MW / 6	yes, 70 %	none	> 0.4	2500
Lanier et al. (1986)	NG	0.88 MW / 5	yes, 65 %	none	0.075	2100
Kokkinos (1992)	NG, coal, CWSF	1.8 MW / 3	yes, 40-75 %	none	1.5	-
Hura and Breen (1993)	NG	18 MW / 5	yes, 68 %	yes, 68 %	0.5	2200-2800
Li et al. (1993)	NG, coal	158 MW/ 4	yes, 75 %	yes	-	-
May et al. (1994)	NG	33-172 MW / 8	yes, 60-70 %	none	-	-
Smart and Morgan (1994)	NG, coal, fuel oil	2.5 MW / 10	yes, 85 %	none	0.1	2300
Kicherer et al. (1994)	NG, coal, fuel oil	0.5 MW / 8	yes, 75 %	none	1.1	-
Mereb and Wendt (1994)	coal	17 kW / 14	yes, 50 %	none	0.18	2200
Payne and Moyeda(1994)	NG	33-158 MW / 4	yes, 50-68 %	yes	0.25-0.5	> 2500
Moyeda et al. (1995)	NG, coal	0.3 MW / 10	yes, 50 %	yes	0.2-0.6	2600

Spliethoff et al. (1996)	methane, syngas	30 kW / 4	yes, 70 %	none	1.2	2400
Liu et al. (1997)	coal	drop-tube	yes, 55 %	none	0.36	2100
Farzan et al. (1997)	NG	60 MW / 6	yes, 71 %	yes	-	-
Rudiger et al. (1995)	biomass, pyro-gas	30 kW / 5	yes, 50 %	none	1 - 2	2200
Ashworth et al. (1997)	NG, coal, CWSF	3 MW / 5	yes, 60-70 %	none	0.42-0.53	2700
Maly et al. (1997)	NG, PC, cws, BM, Orim	0.6 MW / 5	yes, 75 %	none	0.4-0.7	2600
Falcone Miller et al., (1996)	CWSF	30MW / 6	Yes,	None	N/A	N/A
Rostorfer et al. (1998)	Orim	74 MW / 3	yes, 67 %	none	-	-
Kluger et al. (1998)	coal	30 kW / 21	yes, 70 %	none	3	2400
Ashworth et al. (1998)	CWSF	3 MW / 4	yes, 50-77 %	none	0.53	2700

[a] Reburn fuel: NG = natural gas; CWSF = coal-water slurry fuel; PC = pulverized coal; BM = biomass; Orim = orimulsion

[b] RZ – recirculation zone

The primary advantages of reburning over other available NO_x control technologies are that it: 1) provides high levels of NO_x control; 2) can be implemented without significant impact on boiler performance; 3) produces no measurable by-product emissions; and 4) can be applied to all types of boilers, including cyclone-fired boilers, a design that is difficult to adapt to low-NO_x firing configurations. Other notable advantages, other than NO_x control include: SO_2 reduction (Chagger et al., 1997) in proportion to the gas fired (typically 15-20%), reduced ash disposal, also in proportion to the gas fired, reduced maintenance, and improved availability (Folsom, 1994).

The most current reburning techniques rely on using the entire furnace, although the burner fuel-staging concept has been successfully demonstrated (Smart and Morgan, 1994). However, in the current furnace and burner designs using reburning, the required primary, reburn and burnout zones are created by physically separating the three zones within the boiler. This

requires additional expensive operations and it is partly for this reason that the application of reburning on the full scale is currently not more widespread.

Reburning Mechanisms

Mechanisms governing the inter-conversion and destruction of nitrogen species in the fuel-rich reburning zone are the driving force behind reburning technology and have long been the subject of research by several workers (Wendt et al., 1973; Wendt, 1995). Comprehensive parametric studies have been conducted (Chen et al., 1986), delineating the factors that affect reburning effectiveness. Subsequent work by Lanier et al. (1986) identified critical mechanisms controlling the destruction of NO during reburning in a package boiler simulator. The destruction of N_2 by hydrocarbon reactions to form HCN was proposed as a mechanism that would limit the effectiveness of reburning, especially at lower primary NO levels. Using a model that did not account for hydrocarbon reactions, Knill and Morgan (1989) were able to predict the destruction of NO and HCN for selected experiments in an isothermal plug flow reactor. This mechanism was able to predict profiles of all nitrogenous species (NO, HCN and NH_3) in the reburning zone for all tests. Mechanisms governing the destruction of NO in the far fuel rich post flame of a pulverized coal staged combustion system were documented by Bose and Wendt (1988), Mereb and Wendt (1990) and Burch et al. (1994). Their work expands the reburning configuration analysis to predict both HCN and NH_3 concentrations, using measured values of NH_3 in their mechanism.

Alternative Fuels and Coal-Water Slurry Potential as a Reburning Fuel

In the past several years, various testing programs have shown that a wide range of fuels can effectively be used for reburning (Jones, 1997). Coal water slurry (McHale, 1985; Falcone Miller et al., 1996; Huettenhein and Chari, 1998), biomass (Kartak et al., 1996; Juchelkova, 1998) and Orimulsion (Schimmoller, 1998; Rostorfer, et al., 1998) are the ones receiving the highest interest due to their potential for replacing natural gas and coal. Basic reburning performance for coal fuels and biomass were found to be similar or slightly better than that of natural gas, with over 70 % NO_x reduction available at reburn heat inputs above 20 % (Maly et al., 1997). While reburning with alternative fuels has the potential to have boiler impacts, such as increased slagging with biomass, these impacts are generally minimized because the reburn

fuel comprises only a small fraction of the total boiler heat input. Reburning techniques with these fuels are flexible since they can be readily applied to a wide variety of waste products and off-specification fuels having low cost. Therefore, alternative fuel reburning can provide great economic benefits while offering the potential for high levels of NO_x reduction for a wide range of new and retrofit power plant applications.

Coal-water slurry fuel (CWSF) has been regarded for many years as an advantageous alternative for coal burning (Battista and Zawadski, 1995; Battista and Ashworth, 1998; Allen and Beal, 1998). It is estimated that there are over two billion tons of coal fines currently stored in active and inactive ponds in the United States (Falcone Miller, et al, 1995). Furthermore, some 50 million additional tons of fines are added to these ponds each year. These stored coal fines are a byproduct stream from coal cleaning plants and represent a significant fuel loss for coal companies and also an additional operating cost and environmental problem as ponds are filled and new pond permits become necessary. However, if the coal pond fines can be economically recovered and used, the material is no longer a liability but represents a significant stockpile of fuel (Falcone Miller, et al, 1995). These coal fines represent a huge energy resource, enough fuel to generate 3,600 MW of electricity every hour for the next 100 years (Ashworth et al., 1997). Hence, recovery of the fines for use as a low solids coal water slurry is a very attractive option from both an economical and an environmental standpoint.

For reburning application, CWSF needs to be of the same quality as that for the wall-fired and tangentially-fired units. With CWSF reburning, NO_x reductions of up to 75% could be obtained on cyclone units (Ashworth et al., 1998). This is important for example to cyclone-fired boiler operators because NO_x emissions from cyclone units range from 1.0 to 2.0 lb/million Btu and there are not many viable options available to reduce emissions to the U.S. EPA regulated limit of 0.86 lb NO_x/million Btu for units greater than 155 MWe. CWSF reburning is applicable to all types of coal-fired boilers and offers electric utilities a potential low cost option to achieve significant NO_x emissions reduction.

3.1.3.4 Test Program

The study was conducted using the DFC described in Section 3.1.1.1 and shown in Figure 3.1.1. Figure 3.1.24 shows the schematic of the Dalavan nozzle that was used to atomize the CWSF. Pulverized coal (PC) was fired through the central pipe of the burner, and CWSF

was injected in Port 2 to simulate the reburn conditions. CWSF was cofired with coal at 0, 10, 20, 30% of the total thermal input. Fifteen tests were performed in the DFC. The baseline flue gas concentration and temperature profile along the combustor were generated for coal firing. A continuous emission monitoring system (CEM) was used to measure O_2, NO_x, and CO at various port levels. Axial oxygen concentration measurements were also obtained.

Experimental Procedure

A nominal firing rate of ≈ 0.5 million (MM) Btu/h was used in the study. Ports were installed as per EPA methods for stack gas sampling for the sulfur oxides evaluation. The CWSF atomizing gun was placed at port 2 for all tests. Combustion air for CWSF was introduced in port 3 during all reburn tests. An atomizing air pressure of 100 psig was used for the CWSF.

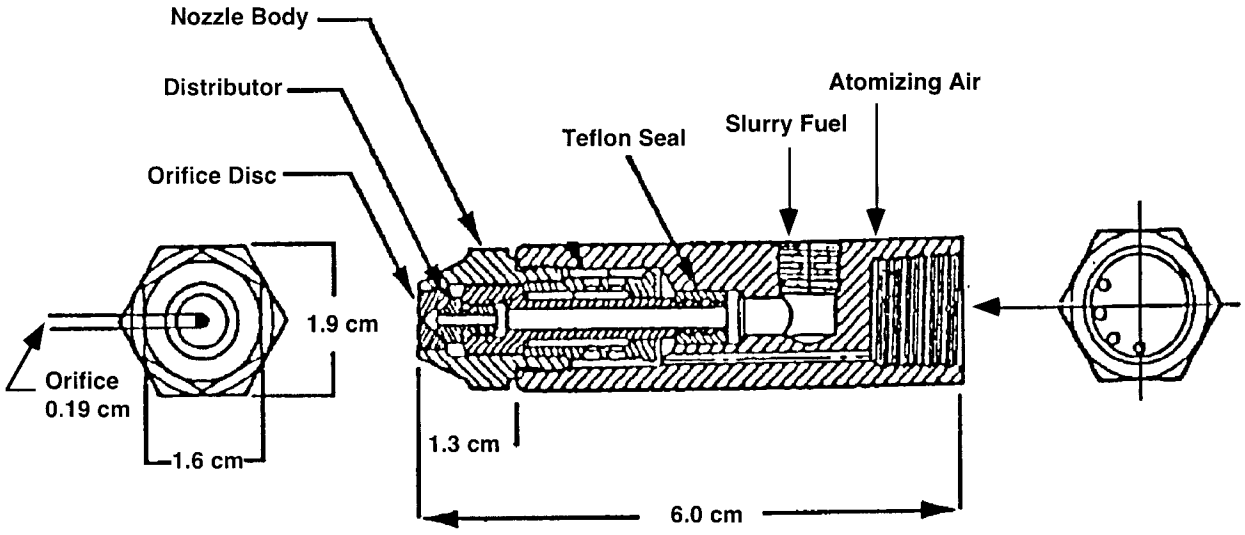

Figure 3.1.24 SCHEMATIC DIAGRAM OF THE DELAVAN NOZZLE

Table 3.1.16 provides a summary of combustion test conditions and emissions data. Data on the gas temperatures using a LAND suction pyrometer, and oxygen, CO, and NO_x concentration profiles using a CEM were also obtained during the tests. Char samples were collected from various ports in the DFC using an isokinetic sampling probe. The char samples were collected in wet condition by washing the probe after each test and were analyzed for carbon, hydrogen, nitrogen and carbon burnout.

Table 3.1.16 Summary of the Test Matrix

Test No.	Thermal Input Slurry (MMBtu/h)	Thermal Input-coal (MMBtu/h)	lb NO_x/ MM Btu	NO_x (corrected, ppm)	Pct. O_2 in the Flue Gas	Comments
1	0.154	0.353	0.71	519	5.39	All combustion air through burner
2	0.151	0.356	0.84	618	4.79	Use 100% PC, 5% O_2 air in burner Port 3, make up air
3	NA[a]	0.357	0.89	654	9.89	100% PC, 0.5 MM Btu air
4	NA	0.360	0.64	469	5.03	5% O_2, 100% PC
5	0.165	0.364	0.83	613	5.26	Use 100% PC, 5% O_2 air in burner Port 3, make up air
6	NA	0.407	0.76	560	5.48	5% O_2, 100% PC
7	NA	0.416	0.94	692	7.91	100% PC, 0.5 MM Btu air
8	0.101	0.410	0.80	587	5.39	All combustion air through burner
9	0.106	0.413	0.93	684	5.49	Use 100% PC, 5% O_2 air in burner Port 3, make up air
10	NA	0.452	0.96	709	6.61	100% PC, 0.5 MM Btu air
11	NA	0.459	0.74	527	5.35	5% O_2, 100% PC
12	0.063	0.457	0.74	541	5.00	All combustion air through burner
13	0.065	0.458	0.87	638	5.38	Use 100% PC, 5% O_2 air in burner Port 3, make up air
14	11.1 lb/h	0.508	0.77	564	5.64	All combustion air through burner
15	NA	0.515	0.89	656	5.00	Baseline test 5% O_2 stack 100% PC

[a] Not Applicable

Analysis of Results

The gas composition (oxygen, CO and NO_x) at various port levels was measured at the center of the combustor, midway between the center and the wall (called "Mid") and at the wall. These profiles are shown in Figure 3.1.25 when firing 100% PC with all the air though the burner. This plot shows that the NO_x concentration in the gas phase was maximum near the burner and as the flue gases passed down the combustor, the NO_x levels decreased. This suggests that the rate of destruction exceeded the rate of production of NO_x. An increase in the destruction is possibly accomplished by the reburn mechanism. Reburning can take place either by homogeneous gas phase reactions or by NO_x - char reactions. Upon heating a coal particle, nitrogen is also distributed between the volatile and char phases. NH_i and HCN species in the volatiles, depending on the temperature, concentration and mixing, can form NO_x or N_2. Simultaneously the char nitrogen will be released to form either NO_x or finally to N_2 as shown in Figure 3.1.26. A balance between the two processes results in a net increase or decrease in the NO_x emissions. Figures 3.1.27-3.1.29 provide NO_x profiles as a function of distance from the

burner when all the air is admitted though the burner, although the amount of fuel is decreased in the case cofiring. This was done in order to keep the amount of air and thus the aerodynamics similar to that of the other tests (especially in the near-burner zone). Figures 3.1.30-3.1.32 show NO_x profiles when cofiring 10, 20, and 30% CWSF but with 90, 80, and 70% of the air respectively, introduced though the burner and the balance introduced through Port 3. It can be seen from Figures 3.1.27-3.1.29 that the initial NO_x levels when cofiring CWSF are lower than the values for 100% PC. This suggests that the formation of NO_x in the initial phases is lower. Subsequently, there is a minor decrease in the NO_x concentration for the tests with CWSF cofiring. These results indicate that the NO_x production and destruction rates, after the primary zone, are almost equal leading to no net production of NO_x.

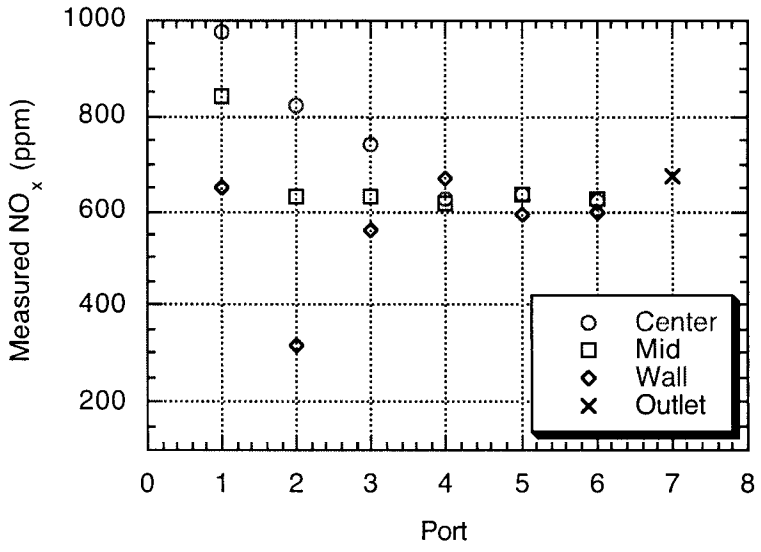

Figure 3.1.25 NO_x PROFILE WHEN FIRING 100% PC WITH ALL OF THE AIR INTRODUCED THROUGH THE BURNER

Conceptually, the reburning process can be divided into three zones: a) the Primary Combustion Zone: This is the main heat release zone which accounts for approximately 80 % of the total heat input to the system and is operated under fuel-lean conditions. The level of NO_x exiting this zone is defined as the input to the reburning process; b) the Reburning Zone: The reburning fuel (10-30 % of the total fuel input) is injected downstream of the primary zone to create a fuel-rich, NO_x -reduction zone. Reactive nitrogen enters this zone from two sources: the primary NO_x input and the fuel nitrogen in the reburning fuel. These reactive nitrogen species

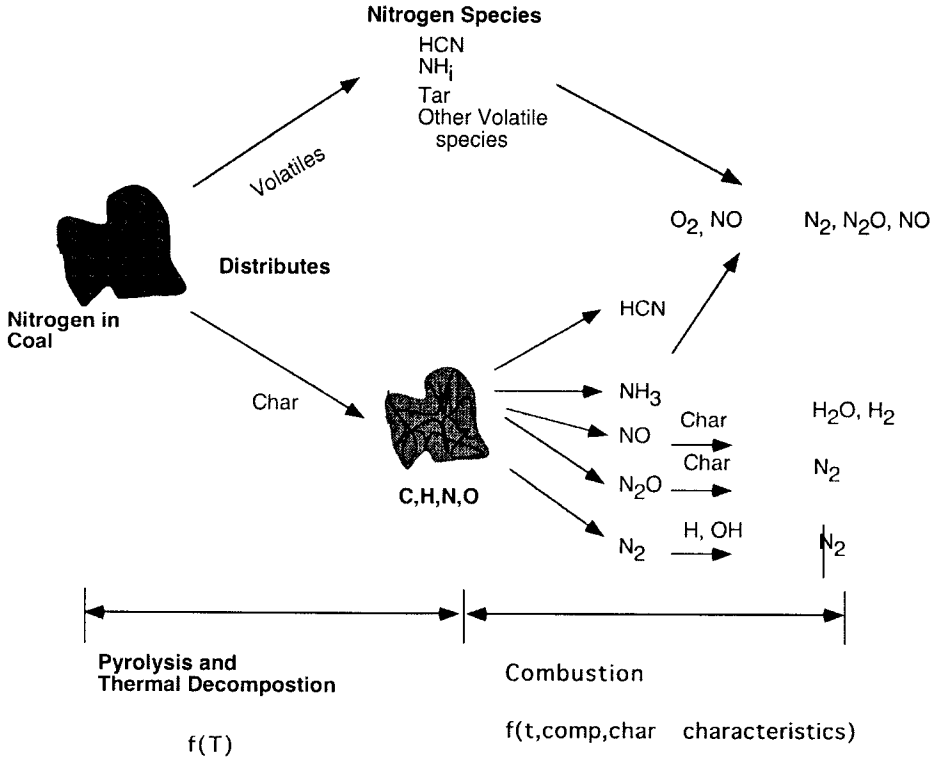

Figure 3.1.26 SCHEMATIC DIAGRAM OF NITROGEN TRANSFORMATIONS DURING PULVERIZED COAL COMBUSTION

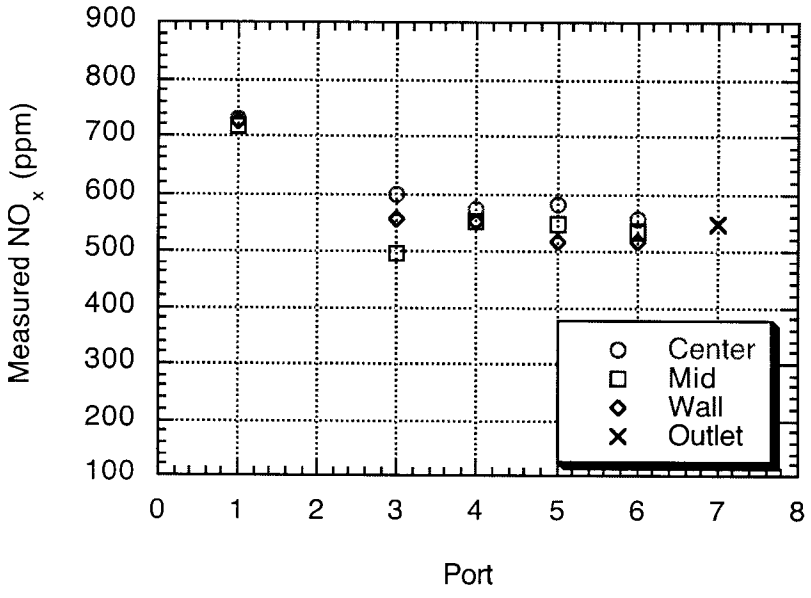

Figure 3.1.27 NO_x PROFILE IN THE COMBUSTOR WHEN FIRING 90% PC AND 10% CWSF WITH ALL OF THE AIR INTRODUCED THROUGH THE BURNER

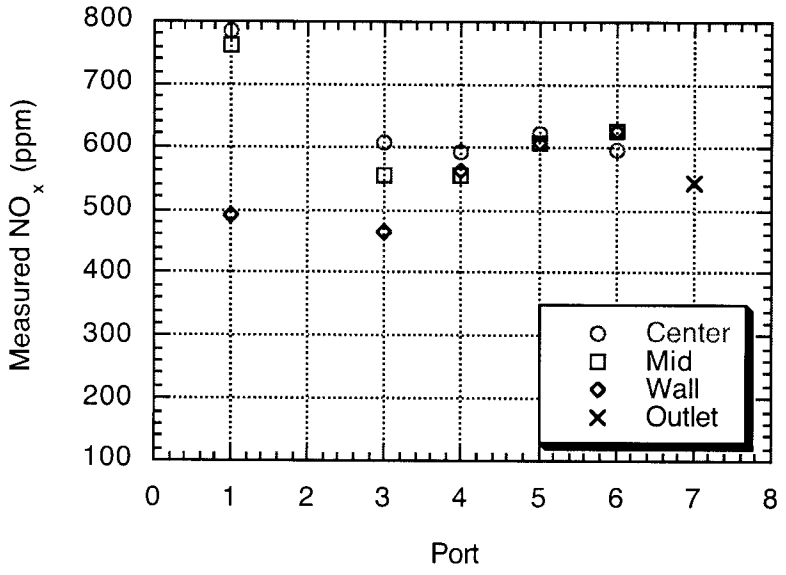

Figure 3.1.28 **NO_x CONCENRATION PROFILE WHEN FIRING 80% PC AND 20% CWSF WITH ALL OF THE AIR INTRODUCED THROUGH THE BURNER**

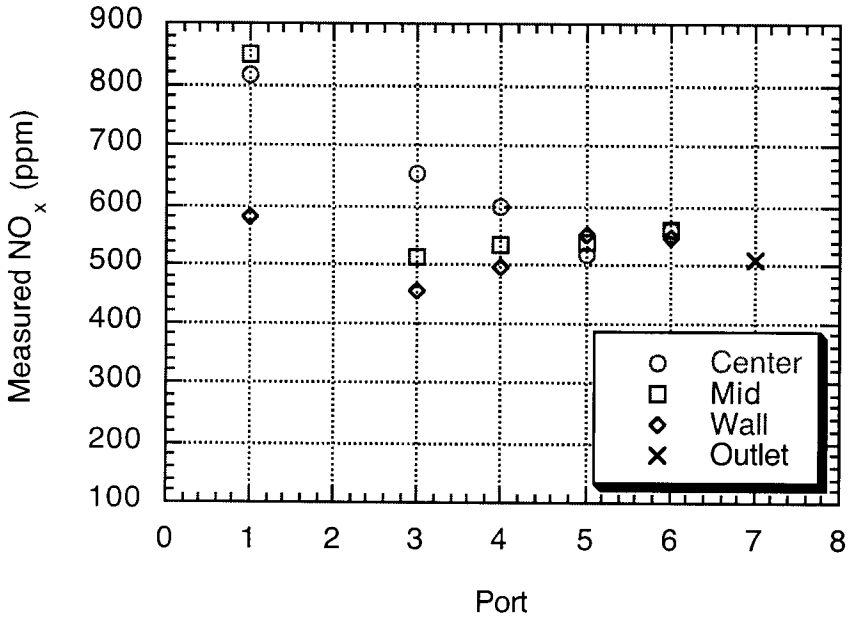

Figure 3.1.29 **NO_x PROFILE WHEN FIRING 70% PC AND 30% CWSF WITH ALL OF THE AIR INTRODUCED THROUGH THE BURNER**

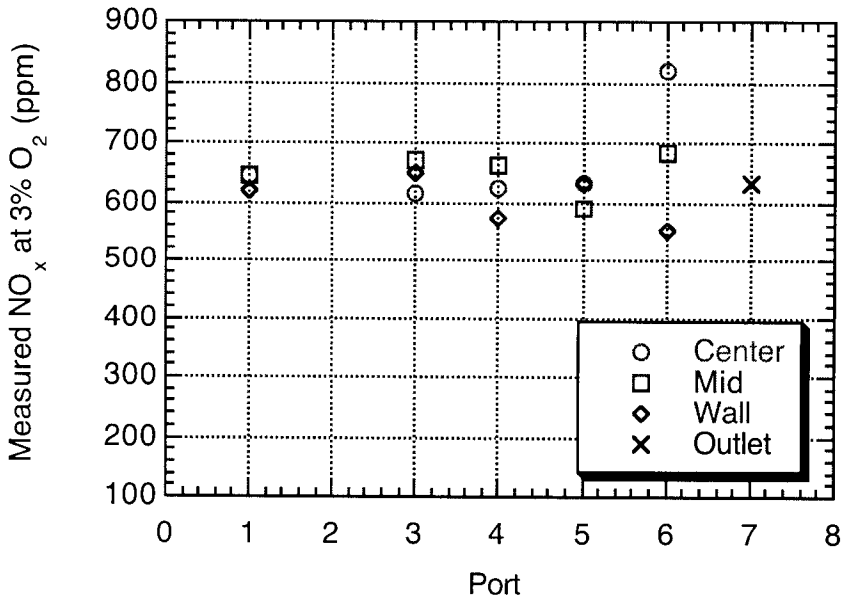

Figure 3.1.30 **NO_x EMISSION PROFILE WHEN FIRING 90% PC AND 10% CWSF WITH MAKE-UP AIR INTRODUCED THROUGH PORT 3**

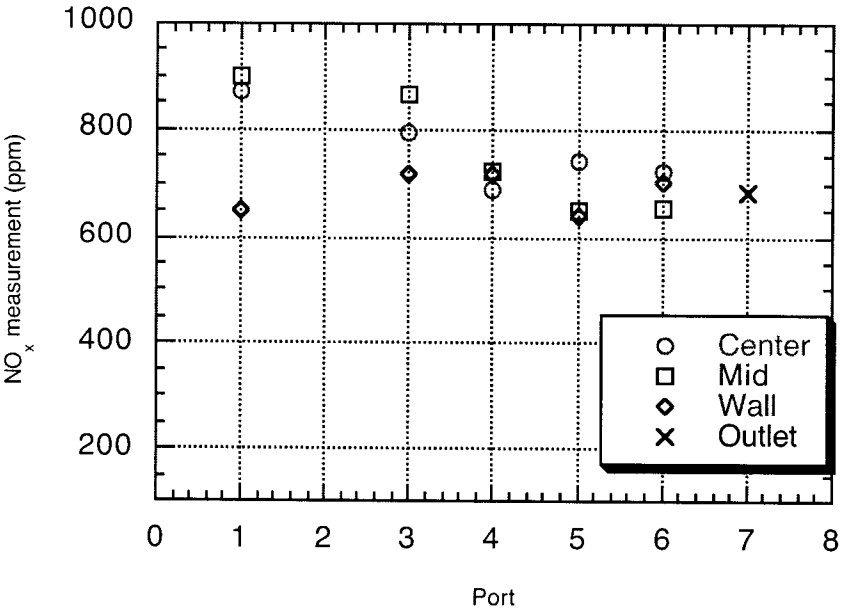

Figure 3.1.31 **NO_x EMISSION PROFILE WHEN FIRING 80% PC AND 20% CWSF WITH MAKE-UP AIR INTRODUCED THROUGH PORT 3**

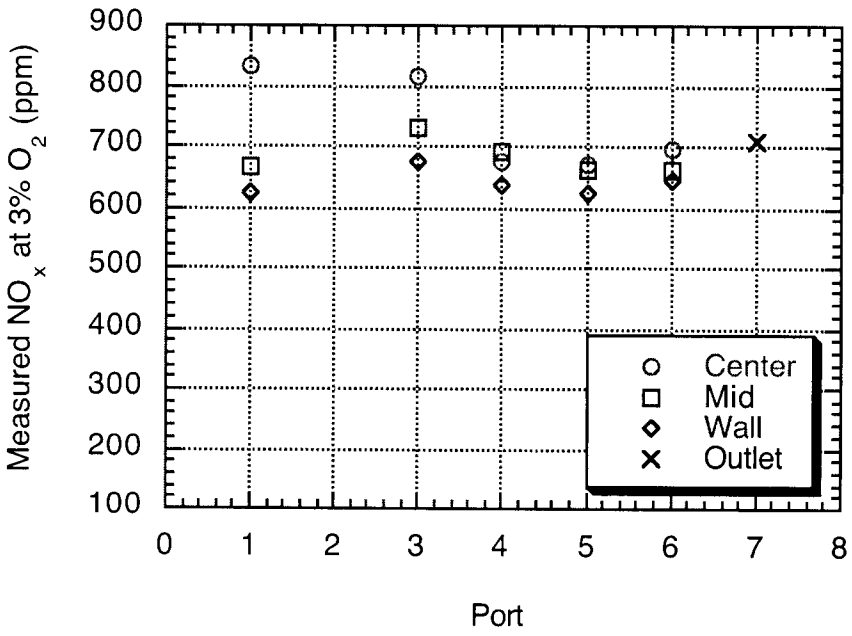

Figure 3.1.32 NO_x EMISSION PROFILE WHEN FIRING 70% PC AND 30% CWSF WITH MAKE-UP AIR INTRODUCED THROUGH PORT 3

react with hydrocarbon radicals, primarily CH from the reburning fuel, to produce intermediate species like NH_3 and HCN (Lanier et al., 1986). The HCN then decays through several reaction intermediates, ultimately producing N_2 via the reverse Zeldovich reaction; and c) the Burnout Zone: In this final zone, air is added to produce overall lean conditions and oxidize all remaining fuel fragments. The total fixed nitrogen species (TFN = NH_3 + HCN + NO + Char N) will either be oxidized to NO_x or reduced to molecular nitrogen.

The amount of nitrogen from the fuel contained in the volatiles and char will change as a function of temperature, nitrogen content and size of the coal particle. Figure 3.1.33 shows the wall temperature profiles for various cofiring configurations. A test was performed with 100% PC but water, equivalent to a 30% CWSF test, was injected in port 3 to separate the effect of NO_x changes due to a temperature decrease and any reburning reactions. Since all the fuel and combustion air was admitted through the burner, the resulting temperature, in the case of 100% PC, was higher than for the rest of the tests. This contributes to higher thermal and fuel NO_x formation in the primary combustion zone. Partitioning of nitrogen between the volatiles and char phase is a function of temperature, heating rate, coal type and equipment used. It has been

shown in the literature that total volatile and nitrogen yields are approximately proportional at comparatively low pyrolysis temperatures (1,800°F) and short heating times, but pyrolysis at temperatures greater than 2,500°F results in the evolution of a significant amount of additional nitrogen (Gibbons et al., 1995). Since the temperature for 100% PC in the Port 1 region is high (>2500 °F), it is likely that more nitrogen is released into the gas phase which, with more air, tends to form higher amounts of NO_x. However, there is a reduction in NO_x concentration between Ports 1 and 3. This is primarily due to gas phase reaction involving hydrocarbon species from the volatiles.

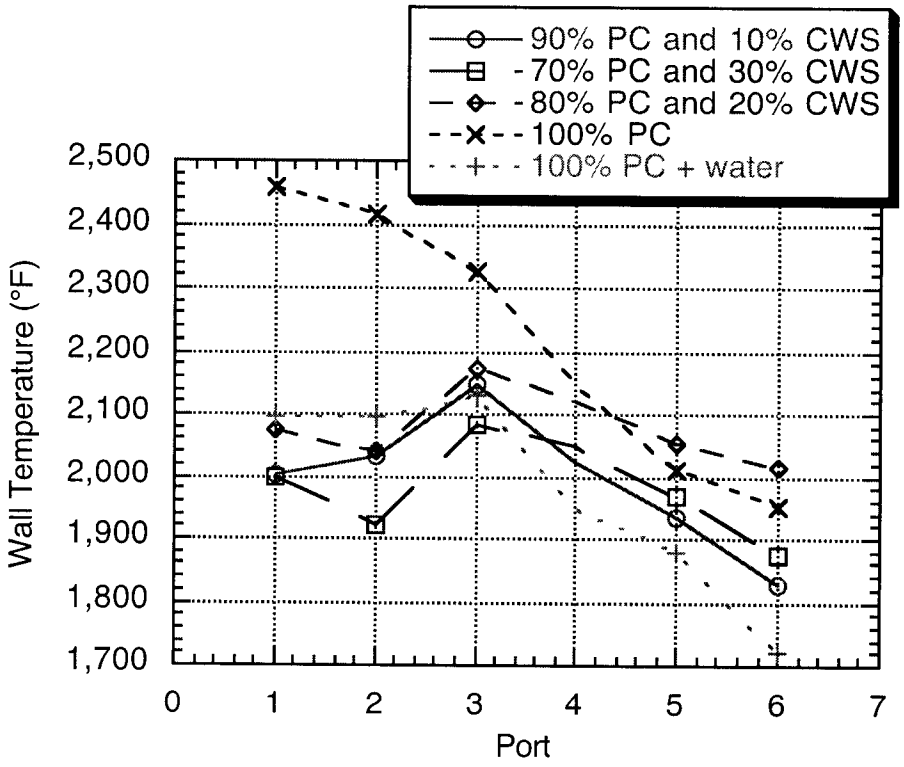

Figure 3.1.33 TEMPERATURE PROFILE FOR VARIOUS COFIRING CONFIGURATIONS

Figure 3.1.34 shows the carbon burnout as a function of distance from the burner. These data were obtained from the isokinetic char samples that were collected during the tests. It is clear that that the carbon burnout during cofiring tests was lower than that for the 100% PC test. This implies that a lesser amount of carbon was available in the form of HC radicals during the initial stages of cofiring than for the 100% PC run. Figure 3.1.35 shows the percentage of

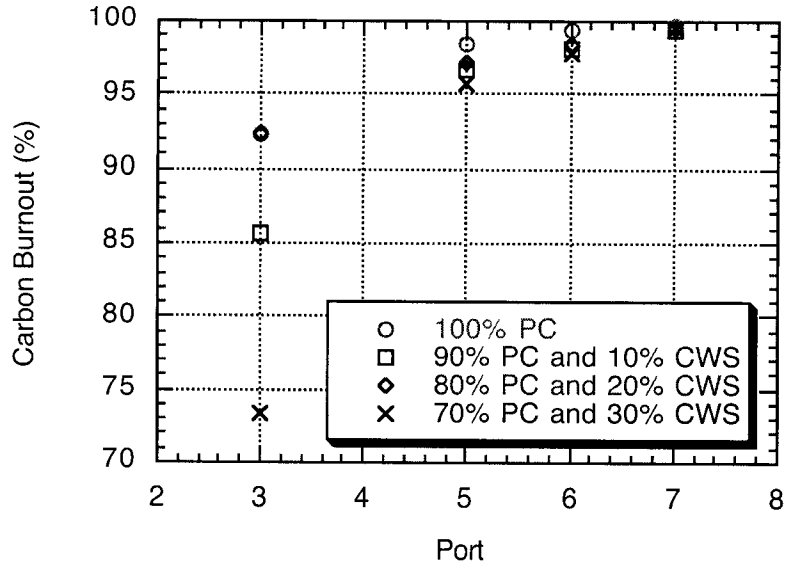

Figure 3.1.34 CARBON BURNOUT AS A FUNCTION OF DISTANCE FROM THE BURNER

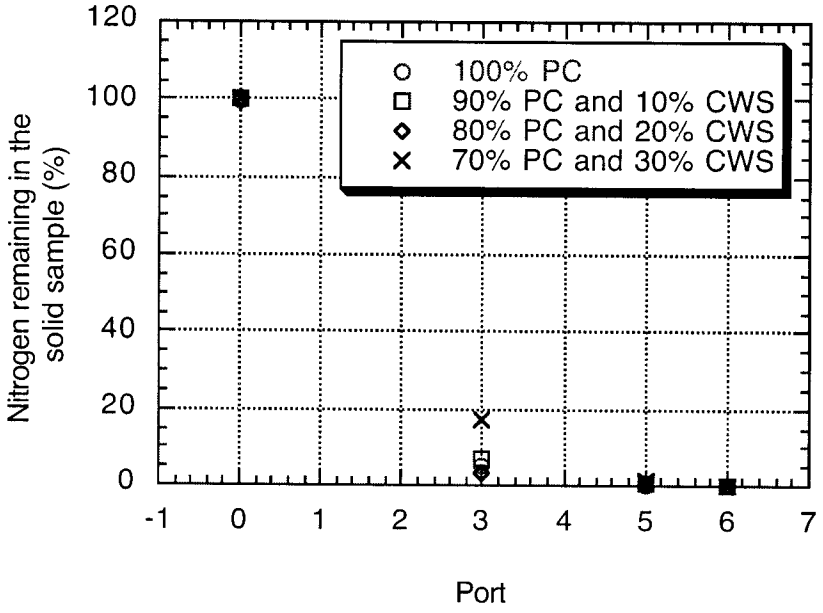

Figure 3.1.35 PERCENT NITROGEN REMAINING IN THE SOLID SAMPLE AS A FUNCTION OF DISTANCE FROM THE BURNER

original nitrogen that remained in the solid phase (char). The chars collected show higher amounts of carbon, and up to 18% of total nitrogen remaining in the char phase at Port 3. Wendt (1995) shows that under rich conditions, HCN plays a critical role in driving the nitrogen cycle to form N_2 and that one source of HCN formation is the destruction of NO by hydrocarbon radicals, which is the main reburning reaction destroying NO. In addition, Lanier et al. (1986) and Mereb and Wendt (1990) have shown that the N_2 fixation reaction also produces HCN, especially under natural gas reburning conditions. Mereb and Wendt (1994) confirmed the fact that reburning with pulverized coal is also effective but less than with gas because natural gas produces more hydrocarbon species in the NO_x-reduction zone and reactions between NO and hydrocarbons are important. Their data showed that with coal reburning, HCN was destroyed more rapidly than it was being formed and its values decayed to levels below 20 ppm within 0.6 seconds. This result supported their hypothesis that it is important to maintain HCN formation rates during long time scales in order to keep N_2 formation mechanisms going, that this formation is mostly due to hydrocarbon reactions with NO or N_2 and that any slow release of nitrogen from the coal residue is a minor contributor to the process. The results in the present study also confirm these observations since the residence time between Ports 1-4 is approximately 0.6-0.7 seconds. The gas phase reburning after this port appears to be insignificant.

NO is expected to be the primary product of char nitrogen combustion (Thomas, 1997). However, the NO-carbon reaction can reduce the NO to N_2. NO reduction is enhanced by the presence of CO (Thomas, 1997). From the CO measurements in the combustor in this study, no significant difference in the CO in the gas phase emissions was observed. In most of the tests the CO concentration was around 100-120 ppm. Therefore, it is likely that the NO produced from oxidation of char nitrogen reacts with the carbon in the pore structure. Char produced from the CWSF is texturally different from char produced from PC (Pisupati et al., 1996). Therefore, local NO-char reactions are responsible for the small reduction in NO above and beyond the reduction obtained due to the temperature reduction caused by water addition.

The reburning zone stoichiometry is controlled by the reburn fuel heat input and different air staging configurations. Figure 3.1.36 shows the effect of reburn fuel fraction on NO_x reduction for CWSF and other fuels, combined with two different air staging configurations: all combustion air at the burner and make-up air addition downstream at Port 3, respectively. Each

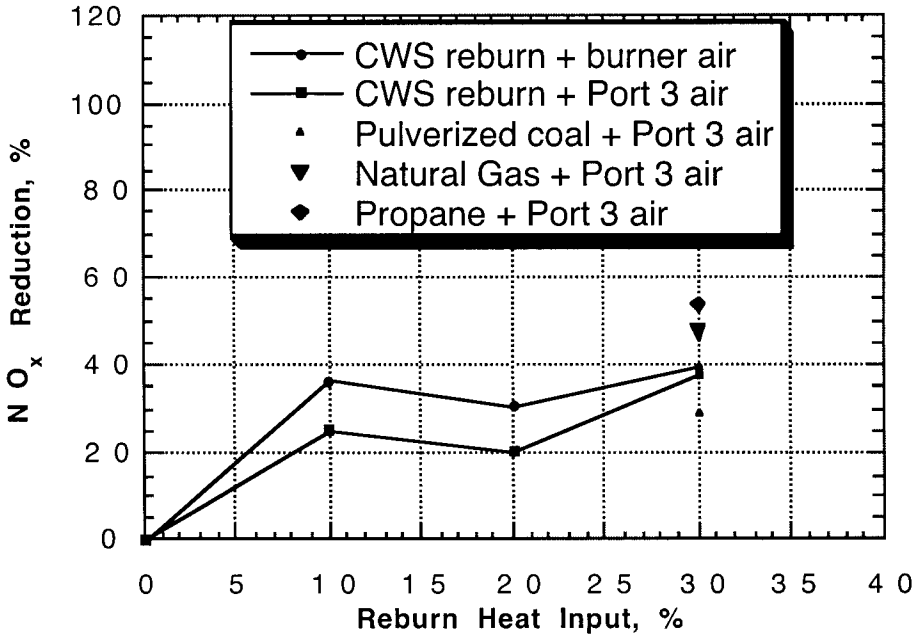

Figure 3.1.36 EFFECT OF REBURN FUEL HEAT INPUT ON NO_x REDUCTION FOR DIFFERENT FUELS AND AIR-STAGING CONFIGURATIONS

separate case proved effective in NO_x reduction, with reduction levels between 20 and 40 %. Propane and natural gas are the most effective reburn fuels at the same residence times because they need no time for devolatilization. The CWSF and pulverized coal are also effective in reducing NO_x from the primary zone; however they are less effective than the gaseous fuels, most likely because they add additional reactive fuel nitrogen. The maximum NO_x reduction for CWSF was achieved at 30% reburn fuel input. Reburning combined with burner air staging gave greater NO_x reduction than combined with Port 3 air staging. This may be regarded as a result of changing stoichiometry in the reburning zone due to different air staging configurations. Also, in both CWSF cases, there is a minimum in the NO_x reduction at 20% reburn fuel input. The explanation for this is due to the different stages of the reburning mechanism, as explained by Smart and Morgan (1994). For all the Port 3 air staging tests, the primary fuel was pulverized coal. It can be seen that under the studied test conditions, the effect of reburn fuel type on the NO_x reduction efficiency is important, differences of up to 25% being noticed. Also, it was observed that a greater reduction in NO_x emissions occurred when reburning CWSF fuel than

when injecting the same quantity of water at the same firing rate. This indicates that the reduction in NO_x emissions is not due solely to the lower temperature caused by the water present in the CWSF. The CWSF nitrogen content, volatile matter, and ability to form CH fragments appear to be parameters of most importance.

From Figures 3.1.26-3.1.32, it can be seen that there is a significant difference between the NO_x concentrations measured at the center and the wall. This indicates the lack of mixing for about 7-8 feet in the combustor. If the NO_x molecules do not mix with hydrocarbon radicals, the reduction in NO_x will be reduced. It has been shown (Mereb and Wendt, 1990) that the reburning mechanisms occur in two regimes: one in which fast reactions between NO and hydrocarbons are usually limited by mixing; the other in which reactions have slowed and in which known gas phase chemistry controls. A separate effort was launched to model the fluid dynamics in the combustor and its role in the reduction of NO_x in addition to the homogeneous and heterogeneous phase chemical reactions.

3.1.3.5 Conclusions

The results of this study confirm the potential of CWSF as a reburn fuel for significant NO_x reduction. Basic reburning performance of CWSF was found to be close to that of natural gas, with 39% NO_x reduction achievable at a CWSF reburn heat input of 30%. Reburning effectiveness depends strongly upon the reburn zone stoichiometry, which is controlled by the reburn fuel heat input and by the air staging configuration.

The results indicate that NO_x is produced during initial phases in pulverized coal flames. The NO_x concentration profile indicates that the concentration decreases rapidly by reburning in the gas phase by the radicals in the volatile phase. Excess air levels (air staging) and mixing appeared to be the most important parameters in reducing the NO_x in the primary zone. When CWSF was cofired with coal, the temperature in the upper part of the combustor was lower because of water addition. The NO_x concentration near the Port 1 region of the combustor was also lower. This reduction was attributed to the lower temperature and lower fuel nitrogen split into the gas phase. Reduction of NO_x due to reburning in the primary zone was not observed for the CWSF tests. The carbon burnout was lower for the CWSF cofiring tests. Therefore, lower amounts of carbon were available in the volatile phase to reduce NOx initially. It is believed that